Published by Institute of Physics Publishing for SISSA

Received: *February 1, 2007*
Revised: *March 09, 2007*
Accepted: *May 8, 2007*
Published: *May 23, 2007*

1-3 leptonic mixing and the neutrino oscillograms of the Earth

Evgeny Kh. Akhmedov*

Department of Theoretical Physics, Royal Institute of Technology (KTH), AlbaNova University Center, SE-106 91 Stockholm, Sweden
E-mail: akhmedov@mpi-hd.mpg.de

Michele Maltoni

The Abdus Salam International Centre for Theoretical Physics, Strada Costiera 11, I-34014 Trieste, Italy, and Departamento de Física Teórica & Instituto de Física Teórica, Facultad de Ciencias C-XI, Universidad Autónoma de Madrid, Cantoblanco, E-28049 Madrid, Spain
E-mail: maltoni@delta.ft.uam.es

Alexei Yu. Smirnov

The Abdus Salam International Centre for Theoretical Physics, Strada Costiera 11, I-34014 Trieste, Italy, and Institute for Nuclear Research, Russian Academy of Sciences, Moscow, Russia
E-mail: smirnov@ictp.trieste.it

Abstract: We develop a detailed and comprehensive description of neutrino oscillations driven by the 1-3 mixing in the matter of the Earth. The description is valid for the realistic (PREM) Earth density profile in the whole range of nadir angles and for neutrino energies above 1 GeV. It can be applied to oscillations of atmospheric and accelerator neutrinos. The results are presented in the form of neutrino oscillograms of the Earth, i.e. the contours of equal oscillation probabilities in the neutrino energy-nadir angle plane. A detailed physics interpretation of the oscillograms, which includes the MSW peaks, parametric ridges, local maxima, zeros and saddle points, is given in terms of the amplitude and phase conditions. Precise analytic formulas for the probabilities are obtained. We study the dependence of the oscillation pattern on θ_{13} and find, in particular, that the survival probability $P_{ee} < 1/2$ appears for $\sin^2 2\theta_{13}$ as small as ~ 0.009. We consider the dependence of the oscillation pattern on the matter density profile and comment on the possibility of the oscillation tomography of the Earth.

Keywords: Neutrino Oscillations, Matter Effects, 1-3 Leptonic Mixing.

JHEP05(2007)077

Contents

1. Introduction

Substantial future progress in neutrino physics will be related to the long baseline experiments as well as studies of the cosmic and atmospheric neutrinos. The key element of these experiments is that neutrinos propagate long distances inside the Earth before reaching detectors. Oscillations in the matter of the Earth change flavor properties of neutrino fluxes, which opens up possibilities to

*On leave from the National Research Centre Kurchatov Institute, Moscow, Russia

JHEP05(2007)077

- study dynamics of various oscillation effects;
- determine yet unknown oscillation parameters: 1-3 mixing, deviation of the 2-3 mixing from maximal and its octant, the type of the neutrino mass hierarchy, and CP-violation;
- perform the oscillation tomography of the Earth;
- search for various new effects caused by non-standard neutrino interactions and/or by exotic physics (such as violation of Lorentz or CPT invariance).

The sensitivity of present-day experiments to the corresponding effects, that appear usually as small corrections to the leading oscillation phenomena (e.g. $\nu_\mu \leftrightarrow \nu_\tau$ vacuum oscillations), is rather low. In the case of atmospheric neutrinos this is related to low fluxes and therefore low statistics of events, and also to uncertainties in the fluxes. The accelerator neutrino beams are, in principle, well controlled, however in majority of the projects the baselines are relatively short, whereas the very long baseline experiments (e.g. with neutrino factories) employ high energy neutrinos. This means that the region of energies $E_\nu \sim (3-10)\,\mathrm{GeV}$ and nadir angles $\Theta_\nu = 0 - 70^\circ$, where the most interesting oscillation phenomena occur, is not covered. Therefore one needs to rely on high precision measurements of the suppressed "tails" of these phenomena. The dilemma is whether to study small effects with a number of systematical errors and degeneracies, or develop experimental approaches that will allow to cover the regions of large oscillation effects. The latter option is realized in the concepts of very long baseline accelerator experiments and very large volume atmospheric neutrino detectors.

In connection with possible future experimental developments and discussions of new strategies of research, a detailed and comprehensive study of physics of the neutrino oscillations in the Earth is needed. Some studies in this direction have been carried out in the past.

In the matter of the Earth, the resonance enhancement of $\nu_e \leftrightarrow \nu_{\mu,\tau}$ oscillations can take place [1, 2], with the MSW resonance peak at $E_\nu/\Delta m^2 \sim 2.5 \times 10^3$ GeV/eV^2 [3, 4]. It was also recognized that the size of the Earth is comparable with the neutrino refraction length, and consequently strong enhancement of oscillations can occur for rather deep trajectories (small nadir angles) and not too small mixing angles: $\sin^2 2\theta_{13} > 0.03$. With decreasing baseline, first the matter effect and then the oscillation effect disappear. This phenomenon [1, 5], termed "vacuum mimicking", implies that for short baselines the flavour transitions are described by the vacuum oscillation formula.

For 1-2 mixing the resonance is in the neutrino channel and at rather low energies: $E_\nu \sim 0.1\,\mathrm{GeV}$. For non-zero 1-3 mixing the MSW resonance peak related to the atmospheric mass splitting is at $E_\nu \sim 6\,\mathrm{GeV}$. The peak is narrow and, depending on the mass hierarchy, the enhancement occurs in the neutrino (normal hierarchy) or antineutrino (inverted hierarchy) channels. Possibilities to observe this resonance peak have been explored in connection to the measurements of the mixing angle θ_{13} and determination of the neutrino mass hierarchy [6 – 13]. Furthermore, it was realized that matter effects can also strongly influence $\nu_\mu \leftrightarrow \nu_\tau$ oscillations [14 – 16].

JHEP05(2007)077

A qualitatively new oscillation phenomenon can be realized for neutrinos crossing the core of the Earth due to a sharp change of the density at the border between the core and the mantle [17 – 22]. In particular, for non-zero 1-3 mixing, the existence of an additional peak is predicted in the energy distribution between the peaks due to the MSW resonances in the core and mantle. This core-mantle effect was interpreted as being due to the parametric enhancement of neutrino oscillations [17, 19, 20].[1] The additional peak is a manifestation of the parametric resonance for 3 layers (1.5 period of the "castle wall" profile) in matter [23]. The parametric resonance occurs when the variation of the matter density along the neutrino trajectory is in a certain way correlated with the values of the oscillation parameters [24 – 26]. A different interpretation of this peak, as being due to an interference between the contributions to the oscillation amplitude from different layers of the Earth's mantle and core, has been discussed in [18, 21, 22]. It was uncovered [27] that the parametric resonance condition is fulfilled also at large energies (above the mantle MSW resonance), leading to the appearance of two parametric peaks in the nadir angle distribution. For general consideration of evolution in the multi-layer media, see [28].

Apart from the large scale structures of the density profile, effects of small scale density perturbation have been explored [29].

Analytic approaches have been developed to describe the physics of various oscillation effects, to understand the influence of the density profile modifications on the oscillation probabilities and also to simplify numerical computations. Many studies have been performed in the constant density approximation [3, 4] or approximation of several layers of constant densities [17 – 22, 25, 26, 30, 14, 31]. For the varying densities within the layers a perturbation-theory approach has been developed in [32] for the description of the solar neutrino oscillations in the Earth.

For 3ν mixing the analytic approaches employ various expansions in the small parameters $\sin^2\theta_{13}$ and/or in the ratio of the mass squared differences $\Delta m^2_{21}/\Delta m^2_{31}$ [33]. For the case of non-constant-density matter, different perturbation theory approaches have been developed for oscillations in low density [34, 35] and high density [36, 27] media. In [27] an analytic description of oscillations in the high energy limit has been worked out for the case of the realistic (PREM) density profile. The influence of the Earth density profile on the oscillation probabilities has also been considered in [37].

To some extent, the results obtained so far had fragmentary character. This paper is the first one in a series of papers we devote to a detailed and comprehensive study of oscillations of neutrinos inside the Earth. Here we present a thorough description of neutrino oscillations caused by non-zero 1-3 mixing, with the emphasis on the physics of the phenomenon. In particular, we study the complex pattern and interplay of various oscillation resonances. We perform our study in terms of "neutrino oscillograms" of the Earth: contours of constant oscillation probabilities in the plane of neutrino energy and nadir angle. These plots have been presented in several earlier publications as illustrations [21, 8, 38]. Here we use them as the main tool of the study.

[1] The parametric resonance in neutrino oscillations in the Earth was first discussed for $\nu_\mu \leftrightarrow \nu_s$ oscillations of atmospheric neutrinos in [17], though the parametric peak appeared in some early numerical computations [3, 4].

JHEP05(2007)077

The knowledge of the oscillograms and their properties will allow us to identify the regions of sensitivity of the oscillation probabilities to various neutrino parameters as well as to the Earth density profile, which can help to develop the criteria for the event selections and optimal experimental setups.

In this paper we:

(i) identify the generic structures of the oscillograms and reveal their physical origin;

(ii) introduce the amplitude and phase conditions, which are generalizations of the maximal amplitude and odd-π phase conditions for oscillations in vacuum or constant-density matter to the case of several matter layers of varying densities. We show that these generalized conditions have several different realizations;

(iii) show that the positions of all the important structures in the oscillograms are determined by the different realizations of the generalized amplitude and phase conditions. We also present analytic formulas for these conditions, which allows us to describe the dependence of the structures on yet unknown neutrino parameters, such as θ_{13}, and on the parameters characterizing the Earth density profile;

(iv) present, using these conditions, a complete physics interpretation of the oscillograms. We also discuss the oscillation curves (the spatial dependence of the oscillation probabilities) for the relevant values of the oscillation parameters and give their graphical interpretation in terms of the analogy between neutrino oscillations and spin precession in a magnetic field;

(v) propose an accurate description of the oscillation probabilities based on perturbation theory in deviation of density within the matter layers from the constant ones, following a similar description proposed for low energy solar neutrinos. We obtain analytic expressions (in terms of several known functions) and produce the oscillograms using this approximation;

(vi) study the dependence of the oscillograms on the 1-3 mixing, on the parameters of the density profile of the Earth and on the channel of oscillations.

The paper is organized as follows. In section 2, after some generalities, we introduce the neutrino oscillograms of the Earth, concentrating mainly on $\nu_e \leftrightarrow \nu_{\mu,\tau}$ transitions. We discuss the accuracy of the constant-density-layers approximation of the Earth matter profile and describe the graphical representation of the flavour conversion. In section 3 we give the physics interpretation of the oscillograms. In section 4 we derive approximate analytic formulas for oscillation probabilities for a realistic matter density profile of the Earth. In section 5 we study the dependence of the oscillograms on the 1-3 mixing and on the Earth density profile, and we discuss the oscillation probabilities for the other oscillation channels. Discussion and conclusions follow in section 6.

JHEP05(2007)077

2. Neutrino oscillograms of the Earth

2.1 Context. Evolution matrix

We consider the three-flavor neutrino system with the state vector $\nu_f \equiv (\nu_e,\, \nu_\mu,\, \nu_\tau)^T$. Its evolution in matter is described by the equation

$$i\frac{d\nu_f}{dx} = \left(\frac{UM^2U^\dagger}{2E_\nu} + \hat{V}(x)\right)\nu_f\,, \tag{2.1}$$

where E_ν is the neutrino energy and $M^2 \equiv \mathrm{diag}(0,\, \Delta m^2_{21},\, \Delta m^2_{31})$ is the diagonal matrix of neutrino mass squared differences. $\hat{V}(x) \equiv \mathrm{diag}(V(x),\, 0,\, 0)$ is the matrix of matter-induced neutrino potentials with $V(x) \equiv \sqrt{2}G_F N_e(x)$, G_F and $N_e(x)$ being the Fermi constant and the electron number density, respectively. The mixing matrix U defined through $\nu_f = U\nu_m$, where $\nu_m = (\nu_1,\, \nu_2,\, \nu_3)^T$ is the vector of neutrino mass eigenstates, can be parameterized as

$$U = U_{23}I_\delta U_{13}I_{-\delta}U_{12}\,. \tag{2.2}$$

Here the matrices $U_{ij} = U_{ij}(\theta_{ij})$ describe rotations in the ij-planes by the angles θ_{ij}, and $I_\delta \equiv \mathrm{diag}(1,\, 1,\, e^{i\delta})$, where δ is the Dirac-type CP-violating phase.

Let us introduce the evolution matrix (the matrix of transition and survival amplitudes) $S(x, x_0)$, which describes the evolution of the neutrino state over a finite distance: from x_0 to x. To simplify the presentation, throughout the paper we will use the notation $S(x) \equiv S(x, 0)$ and $S \equiv S(L)$, where L is the total length of the trajectory. The matrix $S(x)$ satisfies the same evolution equation as the state vector (2.1):

$$i\frac{dS(x)}{dx} = H(x)\,S(x)\,. \tag{2.3}$$

The solution of equation (2.3) with the initial condition $S(0) = \mathbb{1}$ can be formally written as

$$S(x) = T\exp\left(-i\int_0^x H\,dx\right)\,. \tag{2.4}$$

It is convenient to consider the evolution of the neutrino system in the propagation basis, $\tilde{\nu} = (\nu_e,\, \tilde{\nu}_2,\, \tilde{\nu}_3)^T$, defined through the relation

$$\nu_f = U_{23}I_\delta\tilde{\nu}\,. \tag{2.5}$$

As follows from (2.1) and (2.2), the Hamiltonian $\tilde{H}$, that describes the evolution of the neutrino vector of state $\tilde{\nu}$, is

$$\tilde{H}(x) = \frac{1}{2E_\nu}U_{13}U_{12}M^2U_{12}^\dagger U_{13}^\dagger + \hat{V}(x)\,. \tag{2.6}$$

This Hamiltonian does not depend on the 2-3 mixing and CP-violating phase. The dependence on these parameters appears when one projects the initial state on the propagation

basis and the final state back onto the original flavor basis. Explicitly, the Hamiltonian $\tilde{H}$ reads

$$\tilde{H}(x) = \frac{\Delta m^2_{31}}{2E_\nu} \begin{pmatrix} s^2_{13} + s^2_{12}\, c^2_{13}\, r_\Delta + 2V(x)E_\nu/\Delta m^2_{31} & s_{12}\, c_{12}\, c_{13}\, r_\Delta & s_{13}\, c_{13}(1 - s^2_{12}\, r_\Delta) \\ \cdots & c^2_{12}\, r_\Delta & -s_{12}\, c_{12}\, s_{13}\, r_\Delta \\ \cdots & \cdots & c^2_{13} + s^2_{12}\, s^2_{13}\, r_\Delta \end{pmatrix} \tag{2.7}$$

where $c_{ij} \equiv \cos\theta_{ij}$, $s_{ij} \equiv \sin\theta_{ij}$ and

$$r_\Delta \equiv \frac{\Delta m^2_{21}}{\Delta m^2_{31}}\,. \tag{2.8}$$

According to (2.5), the evolution matrix $\tilde{S}(x)$ in the basis $(\nu_e, \tilde{\nu}_2, \tilde{\nu}_3)$ is related to $S(x)$ by the transformation:

$$S(x) = \tilde{U}\, \tilde{S}(x)\, \tilde{U}^\dagger, \qquad \tilde{U} \equiv U_{23} I_\delta. \tag{2.9}$$

The evolution of $\tilde{S}(x)$ is given by the equation analogous to eq. (2.3) with the Hamiltonian $\tilde{H}(x)$.

2.2 High energy neutrino approximation

For sufficiently high energies ($E_\nu > 1 - 2\,\mathrm{GeV}$) one can neglect the 1-2 mass splitting. Then, according to (2.7), the state $\tilde{\nu}_2$ decouples from the rest of the system and does not evolve. Therefore, if we parameterize $\tilde{S}$ in the basis $(\nu_e, \tilde{\nu}_2, \tilde{\nu}_3)$ as

$$\tilde{S} = \begin{pmatrix} A_{ee} & A_{e2} & A_{e3} \\ A_{2e} & A_{22} & A_{23} \\ A_{3e} & A_{32} & A_{33} \end{pmatrix} \tag{2.10}$$

we find that in this approximation $A_{e2} = A_{2e} = A_{23} = A_{32} = 0$, $A_{22} = 1$ and the evolution matrix in the flavor basis takes the form

$$S \approx \begin{pmatrix} A_{ee} & s_{23} A_{e3} & c_{23} A_{e3} \\ s_{23} A_{3e} & c^2_{23} A_{22} + s^2_{23} A_{33} & -s_{23} c_{23}(A_{22} - A_{33}) \\ c_{23} A_{3e} & -s_{23} c_{23}(A_{22} - A_{33}) & s^2_{23} A_{22} + c^2_{23} A_{33} \end{pmatrix}, \tag{2.11}$$

where we omitted the CP-phase factor $e^{-i\delta}$ since CP-violating effects are absent in the limit $r_\Delta \to 0$. We will consider the complete 3ν system in the next publication [39]. Denoting by P_A the 2ν transition probability $\nu_e \leftrightarrow \nu_{\mu,\tau}$:

$$P_A \equiv |A_{e3}|^2 = |A_{3e}|^2\,, \tag{2.12}$$

we obtain from (2.11)

$$P(\nu_e \to \nu_e) = 1 - P_A, \tag{2.13}$$

$$P(\nu_e \to \nu_\mu) = P(\nu_\mu \to \nu_e) = s^2_{23} P_A\,, \tag{2.14}$$

$$P(\nu_e \to \nu_\tau) = P(\nu_\tau \to \nu_e) = c^2_{23} P_A\,, \tag{2.15}$$

$$P(\nu_\mu \to \nu_\mu) = 1 - s^4_{23} P_A - 2 s^2_{23} c^2_{23}\, [1 - \mathrm{Re}\, A_{33}]\,, \tag{2.16}$$

$$P(\nu_\tau \to \nu_\tau) = 1 - c^4_{23} P_A - 2 s^2_{23} c^2_{23}\, [1 - \mathrm{Re}\, A_{33}]\,, \tag{2.17}$$

$$P(\nu_\mu \to \nu_\tau) = P(\nu_\tau \to \nu_\mu) = -s^2_{23}\, c^2_{23}\, P_A + 2 s^2_{23} c^2_{23}\, [1 - \mathrm{Re}\, A_{33}]\,. \tag{2.18}$$

The formulas in eqs. (2.13), (2.18) reproduce the probabilities derived in [20].

Thus, in the approximation $\Delta m^2_{21} = 0$ the dynamical problem is reduced to two flavor evolution problem. Throughout this paper we work in the basis where, for a 2-flavor neutrino system, $H_{11} = -H_{22} = -\cos 2\theta_{13}\Delta m^2/4E + V/2$. This can be always achieved by subtracting from H a matrix proportional to the unit matrix and correspondingly rephasing the neutrino vector of state. This symmetric Hamiltonian is related to the Hamiltonian of the 1-3 subsystem $\tilde{H}^{(13)}$, obtained from eq. (2.7) by taking the limit $r_\Delta = 0$ and removing the decoupled state $\tilde{\nu}_2$, as

$$\tilde{H}^{(13)} = H + \left(\frac{\Delta m^2}{4E_\nu} + \frac{V}{2}\right)\mathbb{1}\,. \tag{2.19}$$

For the 2ν case the unitary evolution matrix can be parameterized as

$$S = \begin{pmatrix} \alpha & \beta \\ -\beta^* & \alpha^* \end{pmatrix}, \qquad |\alpha|^2 + |\beta|^2 = 1. \tag{2.20}$$

For density profiles that are symmetric with respect to the midpoint of the neutrino trajectory (for brevity, symmetric profiles), T invariance leads to the equality of the off-diagonal elements of the evolution matrix, $\beta = -\beta^*$, which means that β is pure imaginary [40].

For a single layer of constant density the solution can be written explicitly:

$$S(x) = \begin{pmatrix} \cos\phi(x) + i\cos 2\theta_m\,\sin\phi(x) & -i\sin 2\theta_m\,\sin\phi(x) \\ -i\sin 2\theta_m\,\sin\phi(x) & \cos\phi(x) - i\cos 2\theta_m\,\sin\phi(x) \end{pmatrix}, \quad \phi(x) \equiv \bar{\omega}\,x\,. \tag{2.21}$$

Here is θ_m is the mixing angle in matter and $\phi(x)$ is the half-phase of oscillations in matter with

$$\bar{\omega} = \omega(\bar{V}) \equiv \sqrt{\left(\cos 2\theta_{13}\frac{\Delta m^2_{31}}{4E_\nu} - \frac{\bar{V}}{2}\right)^2 + \left(\sin 2\theta_{13}\frac{\Delta m^2_{31}}{4E_\nu}\right)^2}\,. \tag{2.22}$$

The moduli squared of the elements of S reproduce the well-known probabilities for oscillations in a uniform medium. Thus, in the notation of eq. (2.20),

$$\alpha = \cos\phi + i\cos 2\theta_m\,\sin\phi\,, \qquad \beta = -i\sin 2\theta_m\,\sin\phi\,. \tag{2.23}$$

In what follows we will generalize this result to the cases of several layers of constant densities and also of changing densities within the layers.

In a non-uniform density medium the adiabatic half-phase of oscillations is defined as

$$\phi(x) \equiv \int_0^x \omega(x')\,dx'\,, \qquad \omega(x) \equiv \omega(V(x))\,. \tag{2.24}$$

2.3 Neutrino oscillograms of the Earth

For given values of $|\Delta m^2_{31}|$, $\sin^2 2\theta_{13}$, and the type of neutrino mass hierarchy, the oscillation probabilities depend on the neutrino energy E_ν and the nadir angle of its trajectory Θ_ν. Therefore a complete description of the oscillation pattern can be given by contours of equal oscillation probabilities in the (E_ν, Θ_ν) plane. We call the resulting figures the *neutrino*

oscillograms of the Earth. The plots of this type were produced for the first time by P. Lipari in 1998 (unpublished) and then appeared in several later publications [21, 8, 38]. Here we will employ this kind of plots as the main tool of our study.

We use in our calculations the matter density distribution inside the Earth, ρ, as given by the PREM model [41]. The number of electrons per nucleon, $Y_e \equiv N_e m_N/\rho$ where m_N is the nucleon mass, equals $Y_e = 0.497$ in the mantle and $Y_e = 0.468$ in the core [32]. For the energies $E_\nu > (1-2)\,\mathrm{GeV}$ the oscillation length in vacuum l_ν exceeds 1000 km, and therefore the effects of smaller-scale density perturbations are averaged out. Furthermore, The density profile experienced by neutrinos along any trajectory inside the Earth is symmetric with respect to the midpoint of the trajectory,[2] so that

$$V(x) = V(L-x), \tag{2.25}$$

where $L = 2R\cos\Theta_\nu$ is the length of the trajectory. As we will see below, to a large extent this feature determines the properties of the oscillation probabilities and the structure of the oscillograms.

For numerical calculations we use the current best-fit value of $\Delta m^2_{31} = 2.5\times10^{-3}\,\mathrm{eV}$; in the case of negligible effects of 1-2 splitting, changing Δm^2_{31} is equivalent to correspondingly rescaling the neutrino energy.

In figure 1 we present the oscillograms for the transition probability P_A for normal mass hierarchy and several values of $\sin^2 2\theta_{13}$. The oscillograms have two regions, separated by $\Theta_\nu = 33.1^\circ$ that corresponds to the nadir angle of the border between the core and the mantle. For $\Theta_\nu < 33.1^\circ$, the neutrino trajectories cross the core of the Earth, so that neutrinos traverse two mantle layers and one core layer. For brevity we call this part the *core domain* of the oscillogram. Conversely, the region $\Theta_\nu > 33.1^\circ$ corresponds to the mantle-only crossing trajectories, and we call it the *mantle domain*. As follows from the figure, there are several salient, generic features of the oscillation picture:

- the MSW resonance pattern (resonance enhancement of the oscillations) for mantle-only crossing trajectories, with the main peak at $E_\nu \sim (5-7)\,\mathrm{GeV}$;
- three parametric resonance ridges in the core domain, at $E_\nu > 3\,\mathrm{GeV}$;
- the MSW resonance pattern in the core domain, $E_\nu < 3\,\mathrm{GeV}$, with the core resonance ridge at $E_\nu = 2.5-2.7\,\mathrm{GeV}$;
- regular oscillatory pattern for low energies: valleys of zero probability and ridges in the mantle domain and more complicated pattern with local maxima and saddle points in the core domain.

The small windings of the contours at $\Theta_\nu = 65^\circ$ and 70° correspond to the borders of the transition zone between the inner and upper mantle, while the windings at $\Theta_\nu = 11^\circ$ are due to the border between the inner and outer core.

[2] We neglect possible short-scale inhomogeneities of the matter density distribution in the Earth which may violate this symmetry.

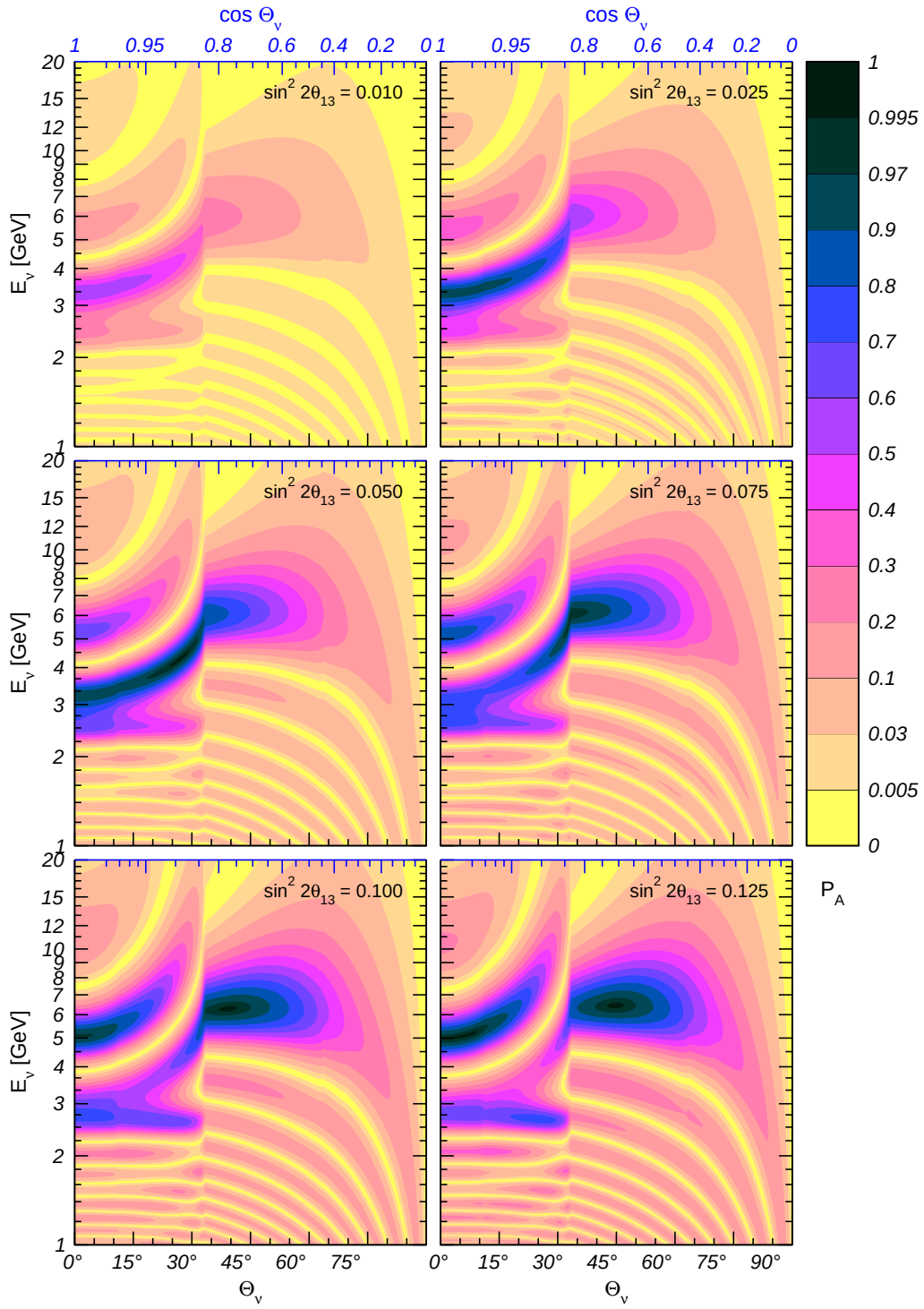

Figure 1: Neutrino oscillograms of the Earth. Shown are the contours of constant probability P_A (edges of the shadowed regions) in the plane of the nadir angle of the neutrino trajectory Θ_ν and neutrino energy E_ν, for different values of the mixing angle θ_{13}.

JHEP05(2007)077

2.4 Constant-density layers approximations

As we shall see, the main features of the oscillograms can be well understood using the approximation of constant-density layers for the density distribution inside the Earth. Furthermore, this consideration allows us to evaluate the sensitivity of the oscillograms to changes of the profile. In figures 2 and 3 we show the oscillograms computed for two different approximations of this kind:

- Approximation of fixed constant-density layers, when the Earth density profile is described by the core and mantle layers of constant densities that are the same for all neutrino trajectories. This approximation has been widely used in the literature. For definiteness, we have taken $\rho_1 = 5.5$ g/cm^3 and $\rho_2 = 11.5$ g/cm^3, which roughly correspond to the average densities in the core and in the mantle. In figure 2 we compare the P_A-oscillograms calculated in this approximation and the exact results. The approximation reproduces the oscillation pattern qualitatively well, with all the features present. However, quantitatively its accuracy is not high above $E_\nu > 3\,\mathrm{GeV}$, in particular, in the resonance region, and for deep trajectories $\Theta_\nu < 60^\circ$. For instance, one can observe an upward shift of the approximate contours compared to the exact ones by about 1 GeV at $E_\nu \simeq (6-10)\,\mathrm{GeV}$. The shift decreases with increasing Θ_ν.

- Approximation of the path-dependent (trajectory-dependent) constant density layers. For each trajectory we find the average potentials $\bar{V}_1$ and $\bar{V}_2$ in the mantle and in the core, respectively,

$$\bar{V}_i(\Theta_\nu) = \frac{1}{L_i(\Theta_\nu)} \int_0^{L_i} V_i(x)\, dx\,, \qquad i = 1, 2, \tag{2.26}$$

  where $L_i(\Theta_\nu)$ is the trajectory length in the i-th layer, and then use the oscillation probability formulas for one or three layers of constant densities. In figure 3 we show the P_A oscillograms calculated in this approximation. One can see that the accuracy of the approximation is noticeably better than that of the fixed-density approximation, especially for the core-crossing trajectories. Again, the largest difference appears for the deep mantle trajectories and $E_\nu > 5\,\mathrm{GeV}$.

As can be seen from figures 2 and 3, the accuracy of the constant-density layers approximations improves with decreasing neutrino energy, the reason being that the matter effects become less important for small E_ν. These approximations also in general work better for the core-crossing trajectories because they are dominated by the evolution in the core and because inside the core the density changes only by about 30%, whereas in the mantle it changes by about a factor of two. For mantle-only crossing trajectories, the approximations work better for shorter trajectories, closer to the surface. Here again the matter effects becomes weaker due to the vacuum mimicking phenomenon [1, 5].

Thus, the approximations of constant-density layers reproduce correctly the qualitative structure of the oscillograms obtained with the realistic PREM density profile of the Earth. All the resonance peaks, ridges and other structures present for the PREM-profile appear

JHEP05(2007)077

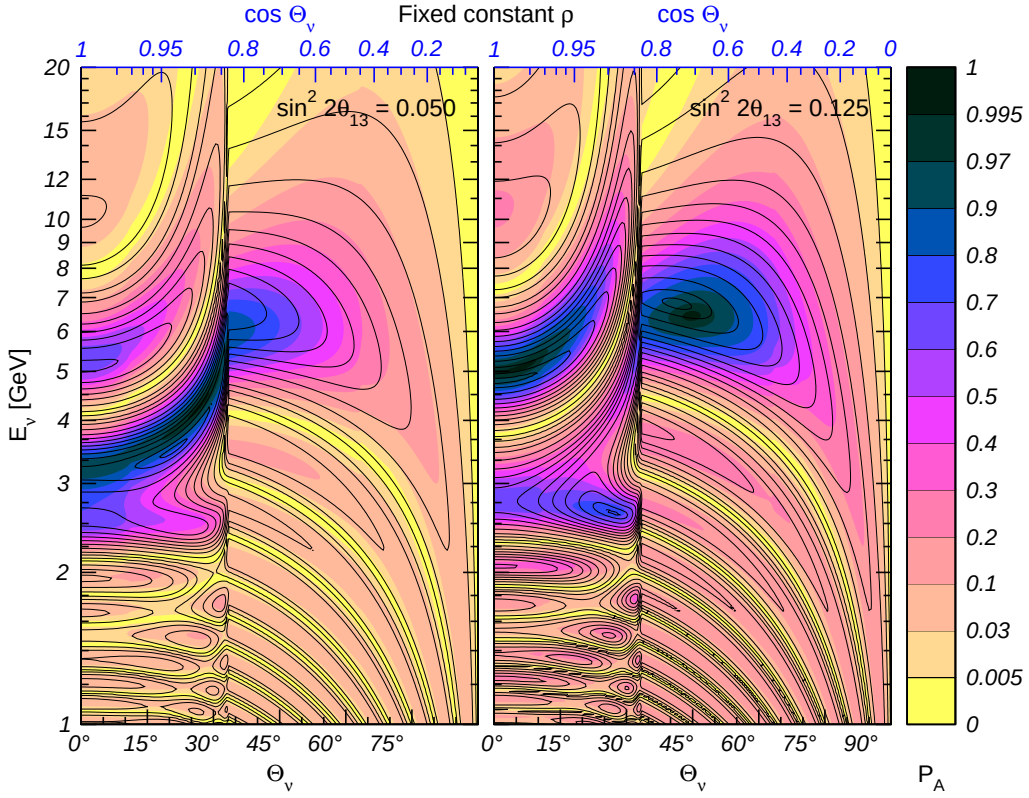

Figure 2: The P_A oscillograms for the PREM density profile (colored regions; grayscale on black-and-white printouts) and for the fixed constant-density layers approximation (black curves).

also in the approximate profile calculations, though their location and shape is not always well reproduced. Therefore one can use these approximations for understanding the main qualitative features of the results for realistic profiles.

2.5 Graphical representation

For illustrative purposes we will use the graphical representation of the 2ν oscillations based on their analogy with spin precession in a magnetic field [3, 42]. Let us introduce the neutrino "spin" vector in the flavor space $\vec{s} = \{s_X,\, s_Y,\, s_Z\}$ with the components

$$s_X(x) = \mathrm{Re}[S^*_{11}(x)\, S_{12}(x)]\,, \quad s_Y(x) = \mathrm{Im}[S^*_{11}(x)\, S_{12}(x)]\,, \quad s_Z(x) = |S_{11}(x)|^2 - \frac{1}{2}\,. \tag{2.27}$$

These components are essentially the elements of the density matrix. The evolution equation for the vector $\vec{s}(x)$ can be obtained from the evolution equation for $S(x)$, given in eq. (2.3):

$$\frac{d\vec{s}}{dx} = 2\,\vec{B}(x) \times \vec{s}(x)\,, \tag{2.28}$$

where

$$\vec{B}(x) = \vec{B}(V(x)) = \frac{\Delta m^2}{4E_\nu}\left\{\sin 2\theta,\ 0,\ \frac{2E_\nu V(x)}{\Delta m^2} - \cos 2\theta\right\}\,. \tag{2.29}$$

JHEP05(2007)077

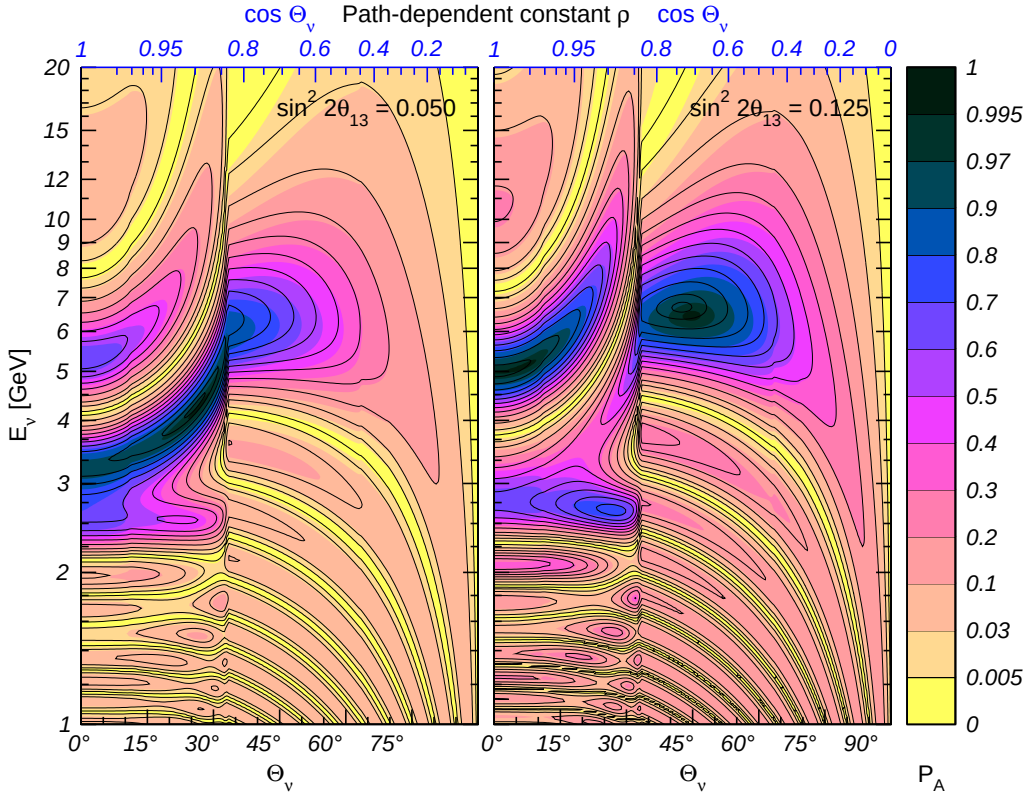

Figure 3: The P_A oscillograms for the PREM density profile (colored regions; grayscale on black-and-white printouts) and for the path-dependent constant-density layers approximation (black curves).

In this representation the oscillations in a medium with constant density is equivalent to a precession of the vector $\vec{s}$ on the surface of the cone (which we will call the precession cone) with the axis $\vec{B}(\bar{V})$ and the opening angle $2\theta_m$. According to eq. (2.29) the axis of the cone is located in the (X, Z) plane and the angle between the cone axis and the Z axis equals $2\theta_m$. In a medium with non-constant density profile the cone axis turns following the change of the angle $2\theta_m(V(x))$. The opening angle of the cone does not change in the adiabatic case, and it changes if the adiabaticity is broken.

3. Physics interpretation of the oscillograms

In this section we give a physics interpretation and description of the four main structures of the oscillograms mentioned in section 2.3, as well as of the contours of zero probability. We show that the positions of the main structures of the oscillograms are described by various realizations of just two conditions: the generalized amplitude and phase conditions.

3.1 Resonance enhancement of oscillations in the mantle

The oscillation pattern in the mantle is determined by the resonance enhancement of the

JHEP05(2007)077

oscillations [1, 2]. In the constant-density approximation, for a given Θ_ν the probability P_A is an oscillatory function of energy, which is inscribed in the resonance curve $\sin^2 2\theta_m(E_\nu)$. The position of the maximum of the resonance peak is given by the MSW resonance condition:

$$E_\nu = E_R(\Theta_\nu) = \frac{\Delta m^2_{31} \cos 2\theta_{13}}{2\bar{V}_1(\Theta_\nu)}\,, \tag{3.1}$$

where $\bar{V}_1(\Theta_\nu)$ is the average value of the potential along the trajectory characterized by Θ_ν (see eq. (2.26)). Eq. (3.1) determines the resonance line in the $(E_\nu,\, \Theta_\nu)$ plane. With the increase of Θ_ν the average potential decreases and consequently E_R increases. According to figure 1, for the MSW resonance in the mantle we have $E_R \sim 6\,\mathrm{GeV}$. The resonance width $\Delta E_\nu/E_R \sim 2\tan 2\theta_{13}$.

The condition $E_\nu = E_R(\Theta_\nu)$ ensures that the amplitude of oscillations is maximal and we will call it the *amplitude* (or *resonance*) *condition*.

Another condition that should be met to obtain the absolute maximum of the transition probability, $P_A = 1$, is the *phase condition*:

$$2\phi(E_\nu, \Theta_\nu) = 2\omega(\bar{V}, E_\nu) L(\Theta_\nu) = (2k+1)\pi \tag{3.2}$$

Since the size of the Earth is comparable with the refraction length in the mantle $l_0 = 2\pi/\bar{V}$, the condition of the absolute maximum (3.2) can only be fulfilled for $k = 0$, i.e. when the length of the neutrino trajectory coincides with the half of the oscillation length in matter. The phase condition (3.2) gives another curve in the $(E_\nu,\, \Theta_\nu)$ plane. The intersection of the resonance line (3.1) and the phase condition line (3.2) determines the position of the absolute maximum of P_A. Combining (3.1) and (3.2) we find that the absolute maximum corresponds to the situation when for the resonance energy the oscillation phase is π:

$$2\omega(\bar{V}, E_R) L(\Theta_\nu) = \pi\,. \tag{3.3}$$

Since $L = 2R\cos\Theta_\nu$ and at the resonance $2\omega = \sin 2\theta_{13}(\Delta m^2_{31}/2E_\nu)$, the condition (3.3) yields

$$\cos\Theta_\nu = \frac{\pi E_\nu}{R \sin 2\theta_{13} \Delta m^2_{31}}\,. \tag{3.4}$$

With the increase of θ_{13} the peak shifts to smaller values of $\cos\Theta_\nu$ (see figure 1). Eq. (3.4) has been used in refs. [15, 11, 12] in discussions of the maximal matter effects and of the determination of the neutrino mass hierarchy.

Let us now reformulate the resonance and the phase conditions for the case of varying density within the mantle. For this we first express these conditions in terms of the elements of the evolution matrix using the explicit results for matter of constant density, eqs. (2.20) and (2.21), and then use the obtained conditions also in the case of varying matter density.

As concerns to the resonance condition, $\cos 2\theta_m = 0$, it can be written according to eqs. (2.20) and (2.23) as $\alpha = \alpha^*$, i.e.

$$S^{(1)}_{11} = S^{(1)}_{22}\,, \tag{3.5}$$

or equivalently,

$$\mathrm{Im}\, S^{(1)}_{11} = 0\,, \tag{3.6}$$

where the superscript indicates the number of layers. This generalization, however, goes beyond the original MSW-resonance condition. For the constant density case it gives

$$\cos 2\theta_m \sin\phi = 0\,. \tag{3.7}$$

This equation has two realizations: the original one

$$\cos 2\theta_m = 0\,, \tag{3.8}$$

and

$$\phi = \pi k, \qquad (k = 1, 2, \ldots) \tag{3.9}$$

and the latter corresponds to $P_A = 0$, which is realized at low energies. In the case of varying density (e.g., in the mantle of the Earth), there is no factorization of the resonance condition (3.6), as in eq. (3.7). However, when the density varies slowly enough along the neutrino path, in certain limits eq. (3.6) is still approximately realized in the form of eqs. (3.8) or (3.9). At low energies the MSW resonance condition is not fulfilled in the Earth's mantle, and therefore the only possible realization of (3.6) is the one in eq. (3.9). In contrast to this, for large energies and small distances eq. (3.9) is not satisfied, and the only way eq. (3.6) can be implemented is through the MSW resonance (3.8). In the intermediate region neither of the two conditions (3.8) and (3.9) is satisfied. Thus, in the resonance region eq. (3.6) interpolates between the MSW resonance condition and the condition $\phi = \pi$.

As for the phase condition, $\phi = \pi/2 + \pi k$, again we can rewrite it in terms of the elements of the evolution matrix, and from eqs. (2.20) and (2.23) we get

$$\mathrm{Re}\,\alpha \equiv \mathrm{Re}\,S^{(1)}_{11} = 0\,. \tag{3.10}$$

The absolute maximum of the transition probability occurs when *both* conditions (3.6) and (3.10) are satisfied simultaneously. In this case $S^{(1)}_{11} = 0$ and $P_A = 1$. This situation corresponds to $\phi = \pi/2$, and from figure 1 we see that it is realized only for $\sin^2 2\theta_{13} \gtrsim 0.08$.

3.2 Parametric ridges and generalized resonance condition

For core-crossing trajectories and $E_\nu > 3\,\mathrm{GeV}$ the oscillatory picture is characterized by three ridges of enhanced oscillation probability. The ridges are the curves along which the probability decreases most slowly from its local or absolute maximum. The lower-energy ridge, which we will call the ridge "A", corresponds to the energies in between those of the MSW resonances in the core and in the mantle, $E_\nu > (3-6)\,\mathrm{GeV}$. It was interpreted in [17, 19, 20] as being due to the parametric enhancement of neutrino oscillations. The other two ridges, "B" and "C", extend above the MSW resonance energy in the mantle. They were also identified as the effects of the parametric enhancement of neutrino oscillations [27]. Here we shall further elaborate on this interpretation.

Recall that the parametric resonance occurs in oscillating systems with varying parameters when the rate of the parameter change is in a special correlation with the values

JHEP05(2007)077

of the parameters themselves. Neutrino oscillations in matter can undergo parametric enhancement if the length and size of the density modulation are correlated in a certain way with neutrino parameters [24, 25].

An example admitting exact analytic solution, and in fact, relevant for our discussion, is the "castle wall" density profile [25, 19]. This is a periodic step function with one period consisting of two layers of widths L_1 and L_2 and electron number densities N_1 and N_2. For 2-flavor neutrino oscillations, the evolution matrix over one period of density modulation (two layers) can be obtained as the product of the evolution matrices for the individual layers, $S^{(2)} = S_2^{(1)} S_1^{(1)}$, where $S_i^{(1)}$ coincides with $S(x)$ given in eq. (2.21). The resulting matrix $S^{(2)}$ can be written as

$$S^{(2)} = Y\mathbb{1} - i\boldsymbol{\sigma}\cdot\mathbf{X}\,, \tag{3.11}$$

where Y and $\mathbf{X} = (X_1,\, X_2,\, X_3)$ are real parameters satisfying $Y^2 + \mathbf{X}^2 = 1$ and σ_i are the Pauli matrices in the flavor space. The oscillation probability for an arbitrary number of layers traversed by neutrinos can be written as a product of the amplitude

$$A = \frac{X_1^2 + X_2^2}{X_1^2 + X_2^2 + X_3^2}\,, \tag{3.12}$$

which does not depend on the number of the layers, and an oscillating factor, which depends on this number [19]. The amplitude A reaches its maximum when $X_3 = 0$, or explicitly [19]

$$X_3 = -(s_1 c_2 \cos 2\theta_1 + s_2 c_1 \cos 2\theta_2) = 0, \tag{3.13}$$

where $s_{1,2} \equiv \sin\phi_{1,2}$ and $c_{1,2} \equiv \cos\phi_{1,2}$. Here $2\phi_{1,2}$ are the oscillation phases acquired in the layers 1 and 2, and $\theta_{1,2}$ are the corresponding mixing angles in matter. Note that in the constant-density limit ($N_1 = N_2$ or $\theta_1 = \theta_2 = \theta_m$) this condition reduces to eq. (3.7) with $\phi = \phi_1 + \phi_2$. For $\sin\phi \neq 1$ it coincides with the MSW resonance condition, which is the maximum amplitude condition for oscillations in a matter of constant density.

As was pointed out above, the Earth density profile seen by neutrinos with core-crossing trajectories can be very well approximated by three layers of constant densities, which is nothing but a piece of the castle wall profile; the layers "1" and "2" have to be identified with the Earth's mantle and core, respectively.

The parametric resonance condition (3.13) can be readily generalized to the case of non-constant densities in the mantle and the core of the Earth, though the generalization is not unique. Indeed, according to (3.11) the condition $X_3 = 0$ can be written in terms of elements of the evolution matrix for two layers as the equality of the diagonal elements:

$$S_{11}^{(2)} = S_{22}^{(2)}. \tag{3.14}$$

We will use this equality for an arbitrary density distribution within the layers and call it *the generalized resonance condition*. Note that parameterization (3.11) of the matrix $S^{(2)}$ implies that the generalized resonance condition can also be formulated as the requirement that the diagonal element of $S^{(2)}$ be real: $\mathrm{Im}\, S_{11}^{(2)} = 0$.

In the right panels of figure 4 we show the curves of the generalized parametric resonance condition. Apparently, all the three parametric ridges are very well described by these curves.

JHEP05(2007)077

3.3 Parametric effects and collinearity condition

Another approach to the generalization of the parametric resonance condition to the case of the layers of non-constant density is based on the consideration of the evolution amplitudes in the individual layers. For the particular case of two layers of constant densities, similar considerations have been presented in [22].

For density profiles consisting of two layers we have

$$S^{(2)} = S_2\, S_1 = \begin{pmatrix} S^{(2)}_{11} & S^{(2)}_{12} \\ -S^{(2)*}_{12} & S^{(2)*}_{11} \end{pmatrix}, \tag{3.15}$$

where

$$S^{(2)}_{11} = \alpha_2\, \alpha_1 - \beta_2\, \beta_1^*\,, \qquad S^{(2)}_{12} = \alpha_2\, \beta_1 + \beta_2\, \alpha_1^*\,, \tag{3.16}$$

and α_i, β_i for each layer have been defined in eq. (2.23). The sum of the two complex numbers in the transition amplitude $S^{(2)}_{12}$ can potentially lead to the largest possible result (if they add in the same phase and not in the anti-phase) if the two contributions to S_{12} have the same complex phase (modulo π):

$$\arg(\alpha_2\beta_1) = \arg(\beta_2\alpha_1^*) \mod(\pi)\,. \tag{3.17}$$

It can also be rewritten as

$$\arg(\alpha_1\alpha_2\beta_1) = \arg(\beta_2) \mod(\pi)\,. \tag{3.18}$$

We shall call this condition the *collinearity condition*. It is an extremality condition for the two-layer transition probability under the constraint of fixed transition probabilities in the individual layers. In other words, if the absolute values $|\beta_i|$ of the transition amplitudes are fixed while their arguments are allowed to vary, the transition probability reaches an extremum when these arguments satisfy (3.17) or (3.18). For a realistic situation (neutrino oscillations in the Earth), changes of E_ν and Θ_ν produce correlated changes of the arguments and the absolute values of the individual amplitudes, and therefore in general the condition (3.17) may not correspond to extrema precisely.

If the layers 1 and 2 have constant densities, then $\alpha_i = c_i + i\cos 2\theta_i\, s_i$, $\beta_i = -i\sin 2\theta_i\, s_i$ (see (2.23)), and the condition in eq. (3.17) reproduces the parametric resonance condition (3.13), i.e. $X_3 = 0$. Under this condition the diagonal elements of $S^{(2)}$ are real; therefore, in the case of constant-density layers the collinearity condition, the generalized resonance condition and the parametric resonance condition coincide.

Denoting by $\chi_{\alpha i}$ and $\chi_{\beta i}$ the arguments of the complex amplitudes α_i and β_i, respectively, one can rewrite the collinearity condition as

$$\chi_{\alpha 1} + \chi_{\alpha 2} = \chi_{\beta 2} - \chi_{\beta 1} \mod(\pi)\,. \tag{3.19}$$

Consider now the case of three layers of in general varying densities. For the elements of the evolution matrix $S^{(3)}$ one obtains

$$S^{(3)}_{11} = \alpha_3\, S^{(2)}_{11} - \beta_3\, S^{(2)*}_{12} = \alpha_3\,\alpha_2\,\alpha_1 - \alpha_3\,\beta_2\,\beta_1^* - \beta_3\,\alpha_2^*\,\beta_1^* - \beta_3\,\beta_2^*\,\alpha_1\,, \tag{3.20}$$

$$S^{(3)}_{12} = \alpha_3\, S^{(2)}_{12} + \beta_3\, S^{(2)*}_{11} = \alpha_3\,\alpha_2\,\beta_1 + \alpha_3\,\beta_2\,\alpha_1^* + \beta_3\,\alpha_2^*\,\alpha_1^* - \beta_3\,\beta_2^*\,\beta_1\,. \tag{3.21}$$

In the case of neutrino oscillations in the Earth, the third layer is just the second mantle layer, and its density profile is the reverse of that of the first layer. The evolution matrix for the third layer is therefore the transpose of that for the first one [40], i.e. $\alpha_3 = \alpha_1$, $\beta_3 = -\beta_1^*$, and the expression for $S_{12}^{(3)}$ can be written as

$$S_{12}^{(3)} = \alpha_1\alpha_2\beta_1 - \alpha_1^*\alpha_2^*\beta_1^* + |\alpha_1|^2\beta_2 + |\beta_1|^2\beta_2^* \,. \tag{3.22}$$

Note that β_2 is pure imaginary because the core density profile is symmetric. Therefore the amplitude $S_{12}^{(3)}$ in eq. (3.22) is also pure imaginary, as it must be because the overall density profile of the Earth is symmetric as well. It is easy to see that if the collinearity condition for two layers (3.18) is satisfied, then not only the full amplitude $S_{12}^{(3)}$, but also *each* of the four terms on the right hand side of eq. (3.22) is pure imaginary. We therefore conclude that if the collinearity condition is satisfied for two layers, then it is automatically satisfied for three layers as well. It should be stressed that this is a consequence of the facts that the density profile of the third layer is the reverse of that of the first layer and that the second layer has a symmetric profile. Once again, the collinearity of all the contributions to the transition amplitude potentially leads to the maximal total transition probability for given transition probabilities in each layer.

For symmetric profiles in each of the two layers (and, in particular, for constant-density layers) the generalized resonance condition and the collinearity condition essentially coincide. For layers of non-symmetric densities, the two conditions differ. As can be seen in the right panels of figure 4, both conditions describe the parametric enhancement ridges in the oscillograms quite well. This is a consequence of the fact that the matter density profiles felt by neutrinos traversing the Earth can be well approximated by path-dependent constant density layers.

3.4 Extrema and saddle points

As has been discussed above, in the constant density case the positions of maxima of the oscillation probability are determined by two conditions: the amplitude condition and the phase condition.

For matter of non-constant density, the collinearity condition or the 2-layer generalized resonance condition can be considered as the generalizations of the *amplitude condition*. Taking into account that the density profile of the Earth's core is symmetric (i.e. $\mathrm{Re}\,\beta_2 = 0$), one can rewrite the collinearity condition (3.18) as

$$\mathrm{Re}(\alpha_1\alpha_2\beta_1) = 0 \,. \tag{3.23}$$

Compared with eq. (3.18), this condition has the practical advantage of not being trivially satisfied for $\beta_2 = 0$, which has no physically relevant implications. For trajectories crossing only the mantle of the Earth, one has to set $\alpha_2 = 1$ in eq. (3.23) and the collinearity condition reduces to $\mathrm{Re}(\alpha_1\beta_1) = 0$. Recall that in the limit of constant matter density in the mantle this latter condition reduces to the condition of maximal mixing in matter (barring $\phi_1 = \pi k$).

The phase condition $\phi = \pi/2 + \pi k$ of the constant-density case can be generalized for varying density by expressing it in terms of the elements of the evolution matrix.

According to (2.23), for one layer and the phase $\phi = \pi/2 + \pi k$ the product of amplitudes $\alpha\beta^* = \pm \sin 2\theta \cos 2\theta$ is real. Therefore, we can generalize the phase condition $\mathrm{Im}(\alpha\beta^*) = 0$ taking instead of α and β the elements of the evolution matrix (amplitudes) for an arbitrary profile:

$$\mathrm{Im}(S_{11}S_{12}^*) = 0. \tag{3.24}$$

Furthermore, since for symmetric density profiles S_{12} is pure imaginary, eq. (3.24) gives

$$\mathrm{Re}\, S_{11} = 0\,, \tag{3.25}$$

i.e., the phase condition is fulfilled when S_{11} is pure imaginary.

In the graphical representation of neutrino oscillations based on their analogy with spin precession in a magnetic field (see section 3.6), eq. (3.24) corresponds to the condition that the neutrino "spin" vector is in the (s_X, s_Z) plane. As can be easily seen, this is equivalent to the requirement that the transition probability be stationary with respect to small variations of the total distance L traveled by neutrinos: $dP_A/dL = 0$.

In the right panels of figure 4 we plot the collinearity (amplitude) condition, the generalized resonance condition and the phase condition for two different values of $\sin^2 2\theta_{13}$. As follows from the figure, the simultaneous fulfillment of the phase and amplitude conditions leads not only to absolute maxima of the transition probability ($P_A = 1$), as in the constant density case, but also to local maxima and saddle points. This is an effect of the multi-layer medium. To figure out why this happens, we will use the explicit results for three layers of constant densities. In this case a straightforward calculation gives [19]

$$S_{11}^{(3)} = Z - iW_3\,, \tag{3.26}$$

where

$$Z = 2c_1 Y - c_2\,, \qquad W_3 = -(2s_1 Y \cos 2\theta_1 + s_2 \cos 2\theta_2)\,, \tag{3.27}$$

and

$$Y = c_1 c_2 - s_1 s_2 \cos 2(\theta_1 - \theta_2)\,. \tag{3.28}$$

with $s_{1,2}$ and $c_{1,2}$ defined after eq. (3.13). Both Z and W_3 are real and therefore the phase condition (3.25) gives $Z = 0$, i.e.:

$$2c_1 Y - c_2 = 0 \qquad \text{(phase condition)}. \tag{3.29}$$

Also in this case

$$P_A = 1 - W_3^2. \tag{3.30}$$

The collinearity condition (3.23) reduces to $\sin 2\theta_1 s_1 X_3 = 0$ for constant density layers, and since $\sin 2\theta_1 \neq 0$, we have

$$s_1 X_3 = 0 \qquad \text{(amplitude condition)}. \tag{3.31}$$

Let us analyze possible realizations of these two conditions. According to (3.29), there are two ways to satisfy the phase condition: (i) $c_1 \neq 0$, $Y = c_2/2c_1$ and (ii) $c_1 = 0$, $c_2 = 0$. The amplitude condition (3.31) also has two realizations: (i) $X_3 = 0$, ($s_1 \neq 0$),

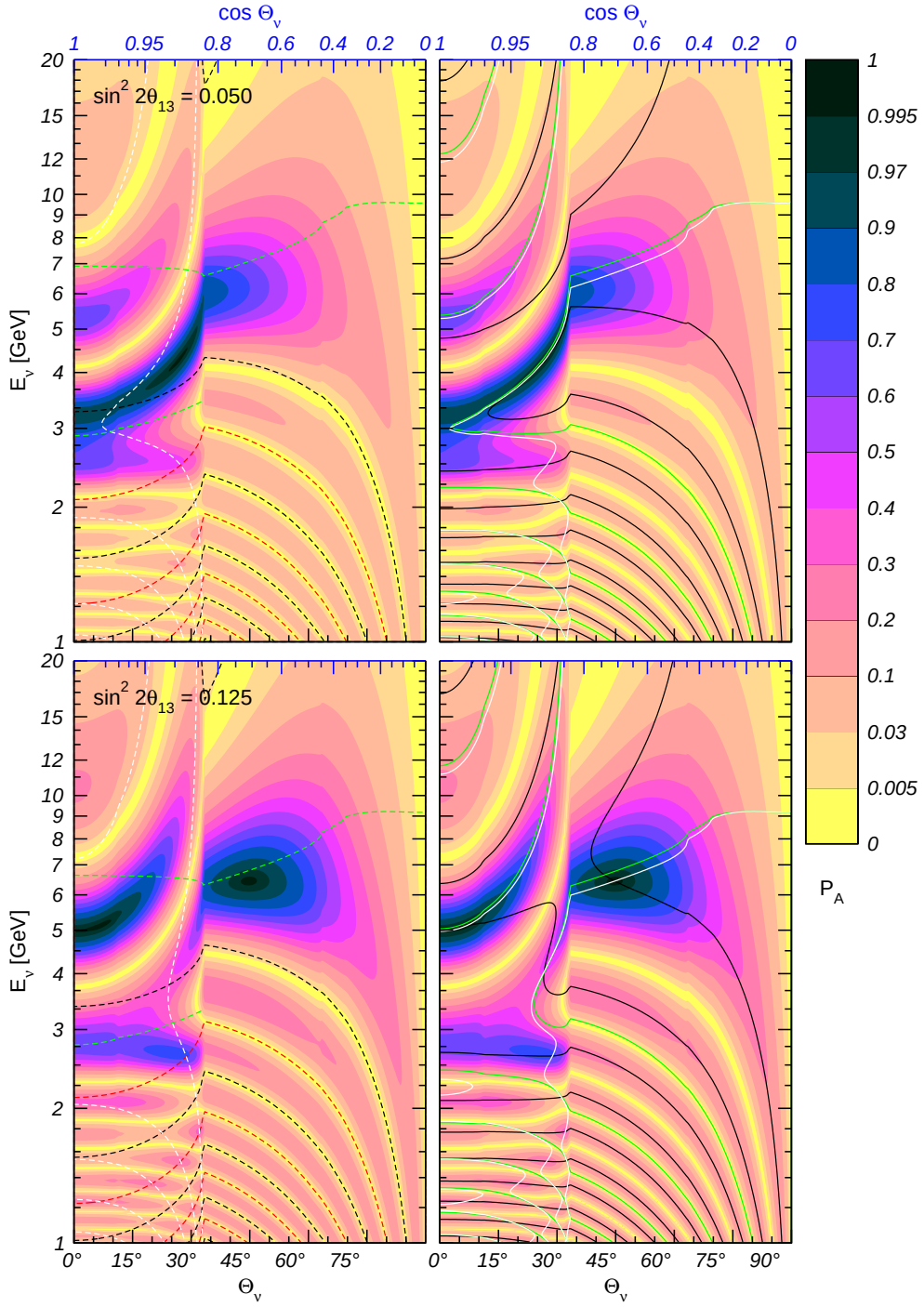

Figure 4: P_A oscillograms and curves of phase and amplitude conditions for the PREM profile. Left panels: the MSW resonance (dashed green), $\mathrm{Re}\,\alpha_1 = 0$ (dashed black), $\mathrm{Im}\,\beta_1 = 0$ (dashed red) and $\mathrm{Re}\,\alpha_2 = 0$ (dashed white). Right panels: collinearity condition (solid white), generalized resonance condition (solid green) and phase condition (solid black).

and (ii) $s_1 = 0$, ($X_3 \neq 0$). As we will see below, different consistent combinations of these realizations lead to absolute maxima, local maxima or saddle points of P_A.

In the non-constant density case, we will use eq. (3.23) as the general amplitude condition and eq. (3.25) as the general phase condition. Using eq. (2.23), we generalize the other equalities discussed above as

$$c_1 = 0 \;\rightarrow\; \mathrm{Re}\,\alpha_1 = 0, \tag{3.32}$$

$$c_2 = 0 \;\rightarrow\; \mathrm{Re}\,\alpha_2 = 0, \tag{3.33}$$

$$s_1 = 0 \;\rightarrow\; \mathrm{Im}\,\beta_1 = 0. \tag{3.34}$$

In the left panels of figure 4 we show the curves that correspond to different conditions. From the constant-density limit it is clear why the curves $\mathrm{Im}\,\beta_1 = 0$ always coincide with some of the amplitude condition curves: this follows from the fact that $\mathrm{Im}\,\beta_1 = 0$ is a particular solution of the amplitude condition.

Let us now consider all consistent realizations of the amplitude and phase conditions, using the terminology of the constant density approximation:

- $X_3 = 0$ ($s_1 \neq 0$) (amplitude); $Y = c_2/2c_1$ ($c_1 \neq 0$) (phase). Plugging this expression for the phase condition in (3.27), we obtain

$$W_3 = \frac{X_3}{c_1}\,. \tag{3.35}$$

  Since $X_3 = 0$ by the amplitude condition, we have $W_3 = 0$ and, consequently, from eq. (3.30) $P_A = 1$. Thus, in the constant density layers approximation a simultaneous fulfillment of the phase and collinearity conditions should lead to $P_A = 1$, provided that $c_1 \neq 0$ or ± 1. This possibility is realized only on the ridge A, at a point where the two curves that correspond to the generalized amplitude and phase conditions cross. The other curves, depicting the conditions (3.32), (3.33) and (3.34), cannot pass through this point. Notice that at this crossing point the oscillation half-phases in the core and mantle differ from $\pi/2$ and π, and there is a nontrivial interplay between the phases and mixing angles in the parametric resonance condition (3.13).

- $c_1 = 0$, $c_2 = 0$ (the latter equality follows from eq. (3.29)) (the phase condition). In this case the amplitude condition, $X_3 = 0$, is satisfied automatically. Using the explicit formulas for Y (3.28), W_3 (3.27) and eq. (3.30), we obtain $Y = \pm\cos 2(\theta_1 - 2\theta_2)$ and

$$P_A = \sin^2(4\theta_1 - 2\theta_2)\,. \tag{3.36}$$

  This case corresponds to the core and mantle half-phases equal to $\pi/2 + \pi k$. It has a simple graphical representation, when it is enough to consider neutrino "spin" vector in the (X, Z) plane (see section 3.6 below). This representation immediately leads to the expression in eq. (3.36) for the transition probability [17], and shows that this probability has a maximum for neutrino energies between those of the core and mantle MSW resonances (where $\cos 2\theta_1 > 0$ and $\cos 2\theta_2 < 0$), provided that

$(\theta_2 - \theta_1) > \pi/4$, and above the MSW resonances, where $\cos 2\theta_{1,2} < 0$. Below the resonances and between the resonances for $(\theta_2 - \theta_1) \leq \pi/4$, eq. (3.36) corresponds to a saddle point of the transition probability. This agrees with the findings in [19].

As follows from figure 4, for $E_\nu < 2.5\,\mathrm{GeV}$ (below the MSW resonance energies) the intersections of the curves $\mathrm{Re}\,\alpha_1 = 0$ and $\mathrm{Re}\,\alpha_2 = 0$ (the analogues of $c_1 = c_2 = 0$ in the case of non-constant densities within the layers) mark the positions of the saddle points. Also in these points the curves that correspond to the general amplitude and phase conditions intersect (since both conditions are fulfilled). At high energies the condition $c_1 = 0$ is not satisfied: the phase in the mantle is below π. Therefore, the maxima of the transition probability are not achieved.

- $s_1 = 0$ ($c_1 = \pm 1$) (the amplitude condition), $Y = 2c_2/c_1$ (the phase condition). The latter equality can be written as $Y = \pm 2c_2$. On the other hand, from the explicit expression for Y (eq. (3.28)) and for $s_1 = 0$ one has $Y = \pm c_2$. Obviously, the two expressions for Y are consistent only if $c_2 = 0$. For $s_1 = c_2 = 0$ we find from (3.27) $W_3 = \pm \cos 2\theta_2$, and consequently,

$$P_A = \sin^2 2\theta_2. \tag{3.37}$$

This realization corresponds to the oscillation half-phase in the mantle equal to π and therefore to the absence of the oscillation effect in the mantle (in the approximation of constant-density matter). The whole oscillation effect is then due to the evolution in the core. The oscillation half-phase in the core is a semi-integer of π ($c_2 = 0$). eq. (3.37) thus simply corresponds to the maximum oscillation probability for a given mixing angle in matter θ_2. At the intersection points of the curves depicting the conditions $s_1 = 0$ and $c_2 = 0$ the probability takes values that correspond to the resonance enhancement of the oscillations in the core. For non-constant density, according to figure 4 (left panels), the intersections of the curves $\mathrm{Im}\,\beta_1 = 0$ and $\mathrm{Re}\,\alpha_2 = 0$ (which are analogues of $s_1 = 0$ and $c_2 = 0$) correspond to local maxima. These points lie at energies below 2.5 GeV. For higher energies, due to the large oscillation lengths, the oscillation half-phase in the mantle is smaller than π and the condition $s_1 = 0$ is not fulfilled.

Notice that along the lines $\mathrm{Im}\,\beta_1 = 0$ (or $\phi_1 \approx \pi k$) the oscillation effects correspond to the resonance enhancement in the core, whereas the saddle points are situated along the lines $\mathrm{Re}\,\alpha_1 = 0$ (or $\phi_1 \approx \pi/2 + \pi k$).

3.5 Absolute minima and maxima of the transition probability

As follows from figure 4, the absolute minima $P_A = 0$ never appear as isolated points in the oscillograms, but always form continuous lines (valleys of zero probability). Such a property (degeneracy of minima) is lifted for non-zero Δm^2_{21} [39]. This is unlike for the absolute maxima, such as the MSW mantle peak or the parametric resonance peak in the core region, where instead the value $P_A = 1$ is reached only at a few isolated points. This

feature is a consequence of the symmetry of the matter density profile of the Earth, and can be readily understood in the following way.

The condition for the absolute minimum, $P_A = 0$, or $S_{12} = 0$, can be written as

$$\mathrm{Re}\, S_{12}(L,0) = 0\,, \qquad \mathrm{Im}\, S_{12}(L,0) = 0\,, \tag{3.38}$$

and for a generic profile the absolute minima are found as the points where the curves corresponding to the two conditions in (3.38) intersect. However, due to the symmetry of the Earth's matter density profile, the condition $\mathrm{Re}\, S_{12}(L) = 0$ is satisfied automatically for all values of E_ν and Θ_ν. Therefore the zeros of P_A simply coincide with the contour curves $\mathrm{Im}\, S_{12}(L) = 0$.

The absolute maxima, $P_A \equiv |S_{12}|^2 = 1$, are realized when $|S_{11}|^2 = 0$, or

$$\mathrm{Re}\, S_{11}(L,0) = 0\,, \qquad \mathrm{Im}\, S_{11}(L,0) = 0\,. \tag{3.39}$$

Since in general $\mathrm{Re}\, S_{11}$ and $\mathrm{Im}\, S_{11}$ are independent and non-trivial functions of E_ν and Θ_ν, the contours that correspond to equalities in (3.39) do not coincide. The absolute maxima occur only at the intersections of the these contours, which explains why such maxima are isolated points.

Another interesting feature of the transition probability P_A is that its dependence on the distance x along a given trajectory exhibits peculiar symmetry properties for trajectories, corresponding to the absolute minima and maxima of $P_A(L)$. Specifically,

- For trajectories, corresponding to the absolute minima ($P_A(L) = 0$),

$$P_A(L - x) = P_A(x)\,. \tag{3.40}$$

  That is, P_A is symmetric with respect to the midpoint of the trajectory $x = L/2$: $P_A(L/2 + z) = P_A(L/2 - z)$, $z \leq L/2$.

- For trajectories, corresponding to the absolute maxima ($P_A(L) = 1$),

$$P_A(L - x) = 1 - P_A(x)\,. \tag{3.41}$$

  This implies that in the middle of the trajectory $P_A(L/2) = 1/2$ and the function $P' \equiv P_A - 1/2$ is antisymmetric with respect to the midpoint: $P'(L/2+z) = -P'(L/2-z)$.

The proof is straightforward. Due to the symmetry of the density profile with respect to the midpoint of the neutrino trajectory, we have for any point x on the trajectory

$$S(L - x, 0) = S^T(L, x), \tag{3.42}$$

which is essentially a consequence of T-invariance of 2-flavour neutrino oscillations [40]. Then, from the definition of the evolution matrix one finds $S(L,0) = S(L,x)\, S(x,0)$, which can be rewritten (using the unitarity of S) as $S(L,x) = S(L,0)\, S(x,0)^\dagger$. Plugging the latter relation into (3.42), we obtain

$$S(L - x, 0) = S^*(x,0)\, S(L,0)\,. \tag{3.43}$$

For the absolute minima, $P_A = 0$, the evolution matrix $S(L,0)$ should be diagonal, and therefore we obtain from eq. (3.43)

$$S(L-x,0) = S^*(x,0) \begin{pmatrix} e^{i\phi_L} & 0 \\ 0 & e^{-i\phi_L} \end{pmatrix}. \tag{3.44}$$

Consequently,

$$P_A(L-x) = \left| S^*_{12}(x,0) e^{-i\phi_L} \right|^2 = P_A(x)\,. \tag{3.45}$$

For the absolute maxima, $P_A(L) = 1$, the matrix $S(L,0)$ should be off-diagonal (see eq. (3.39)) with pure imaginary elements due to the symmetry of the matter density profile. Therefore, using (3.43), one finds

$$S(L-x,0) = S^*(x,0) \begin{pmatrix} 0 & -i \\ -i & 0 \end{pmatrix}, \tag{3.46}$$

and consequently,

$$P_A(L-x) = \left| S^*_{11}(x,0)(-i) \right|^2 = 1 - P_A(x)\,. \tag{3.47}$$

Notice that, according to figure 4, there are no local minima with $P_A \neq 0$.

3.6 Interpretation of the oscillation pattern for core crossing trajectories

The analysis presented in the previous subsections allows one to give a complete physics interpretation of neutrino oscillations in the Earth. Essentially the whole oscillatory pattern that includes the ridges, absolute and local maxima, saddle points and zeros, can be understood on the basis of different realizations of the amplitude and phase conditions. We illustrate neutrino oscillations inside the Earth for core crossing trajectories by figures 5 and 6, and the corresponding graphical representation of the oscillations is given in figures 7b–7f. For comparison, in figure 7a we also show the graphical representation of the oscillations for a trajectory crossing only the mantle of the Earth.

Core ridge. The core resonance ridge is located at $E_\nu \sim (2.5 - 2.8)\,\mathrm{GeV}$. It is of the MSW resonance nature, but is situated below the MSW resonance line in the core: $E_\nu < E_R(\Theta_\nu)$, the reason being that the values of the oscillation half-phase are different from $\pi/2$. The ridge does not coincides with any curve corresponding to the phase or amplitude condition. At one point on the ridge there is an intersection of the curves $\mathrm{Im}\,\beta_1 = 0$ (the mantle half-phase $\phi_1 = \pi$) and the collinearity condition, as well as of the $\mathrm{Re}\,\alpha_2 = 0$ curve, corresponding to the core half-phase $\phi_2 = \pi/2$ (see figure 4). This crossing point corresponds to the local maximum with zero mantle effect and maximal oscillation amplitude in the core.

As follows from figures 5 and 6, the main contribution to the oscillation probability comes from the MSW-enhanced oscillations in the core, though the mantle contribution is not negligible. The detailed picture depends on the value of $\sin^2 2\theta_{13}$.

At $\Theta_\nu = 27^\circ$ (point Z_3) the phase reaches $\phi_2 = \pi/2$ and furthermore $\phi_1 = \pi$. This corresponds to pure core effect. Notice that with increase of Θ_ν the average density decreases

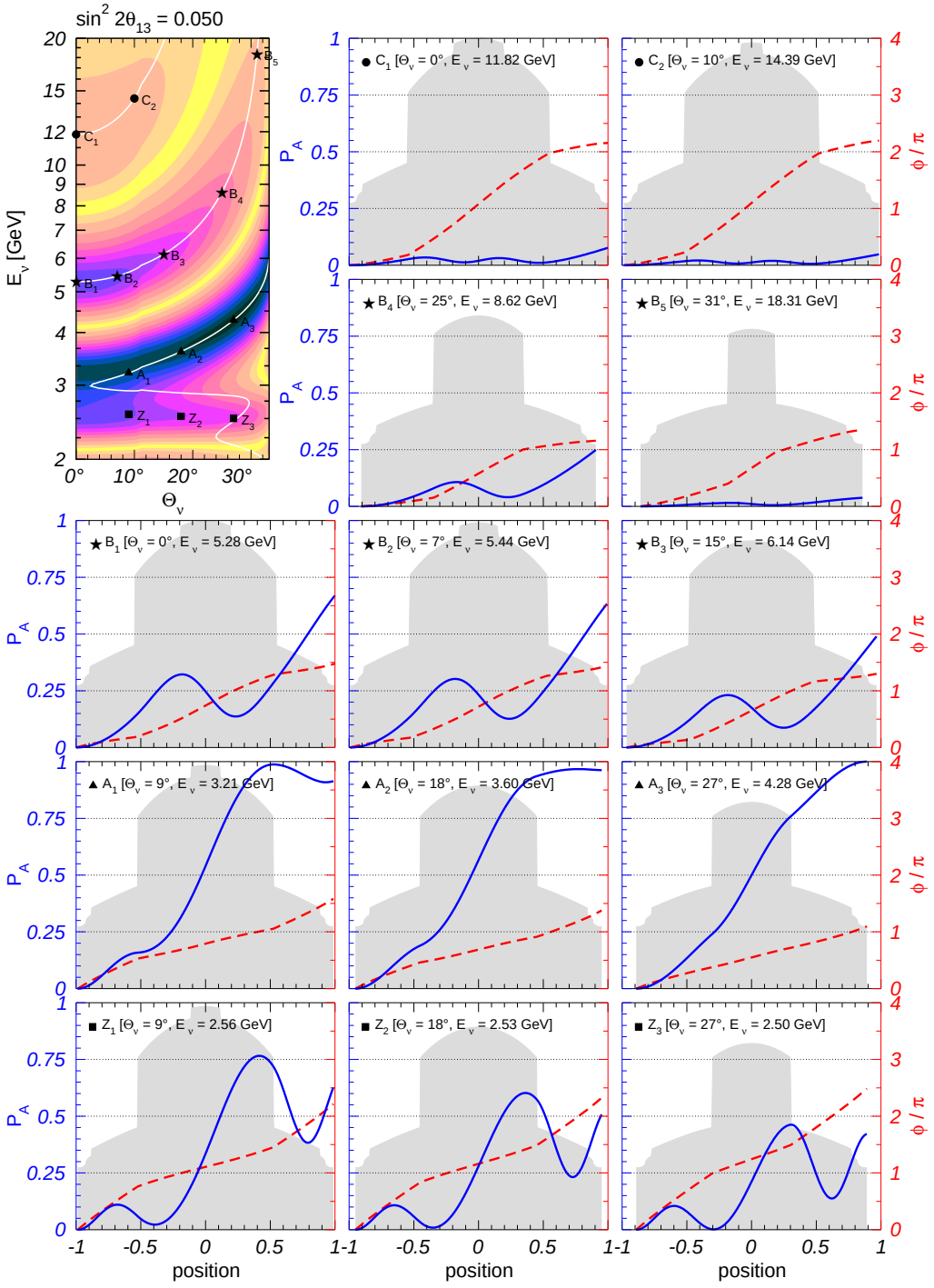

Figure 5: Dependence of the probability P_A (solid blue), half-phase ϕ (dashed red) and the Earth density (gray shade) on the position along the neutrino trajectory, for $\sin^2 2\theta_{13} = 0.05$ and different values of Θ_ν and E_ν. The corresponding points of the oscillogram, together with the curves of the amplitude (collinearity) condition, are shown in the upper-left panel.

JHEP05(2007)077

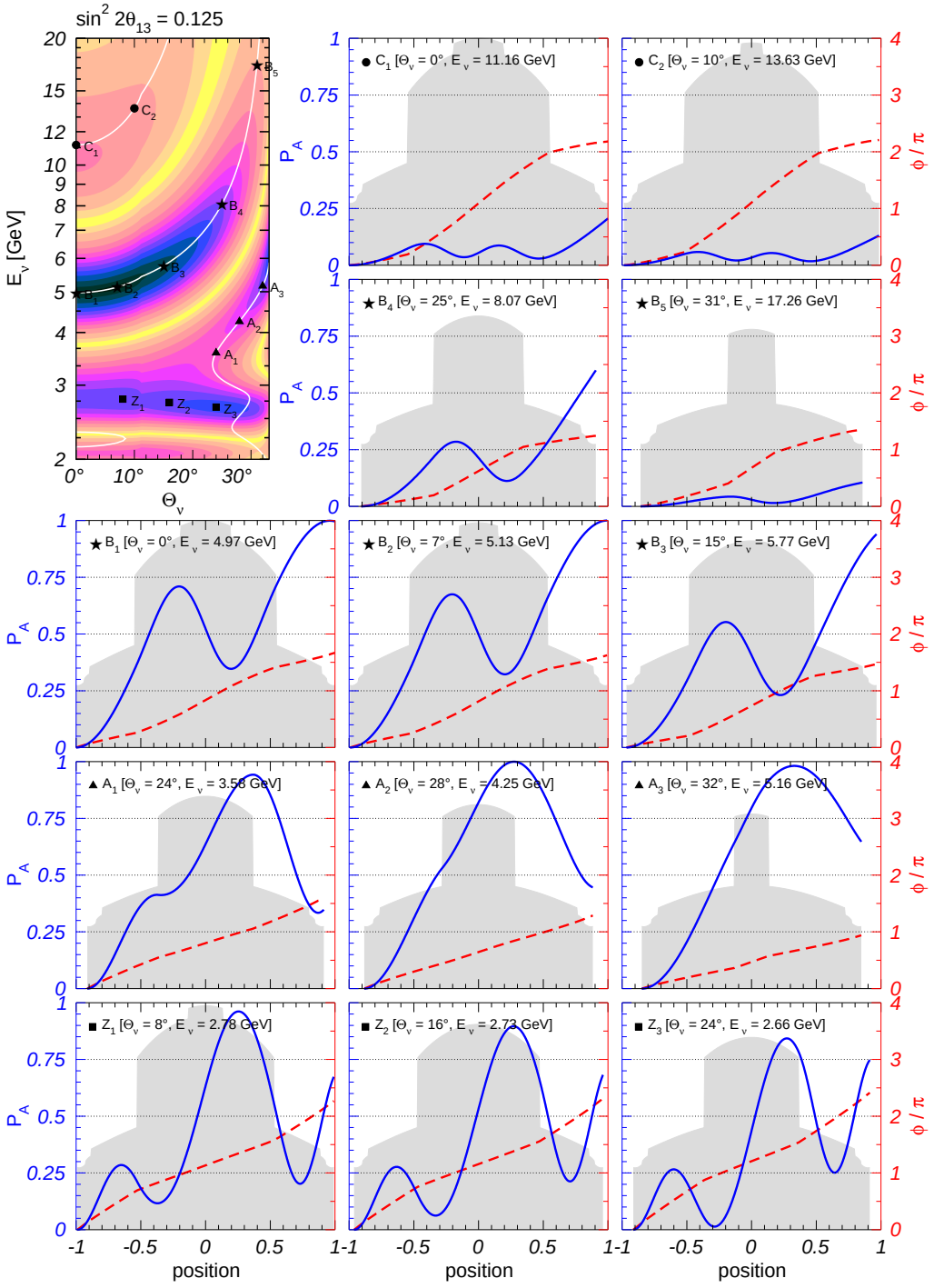

Figure 6: Same as in figure 5, but for $\sin^2 2\theta_{13} = 0.125$.

and the depth of oscillations becomes smaller. In figure 7b we show the graphical representation of evolution with parameters from core-ridge (point Z_3). We show the precession cones in the mantle and in the core in the points close to border between the mantle and

core. Shift of the evolution trajectory from the cone surfaces is due to density change and violation of adiabaticity.

For $\sin^2 2\theta_{13} = 0.05$ another intersection of lines of the amplitude condition and the phase conditions $\mathrm{Re}\,\alpha_2 = 0$ (core half-phase $\pi/2$) occurs at $E_\nu = 3.3\,\mathrm{GeV}$ and $\Theta_\nu = 10^\circ$. Evolution for this configuration is shown in figure 5 point A_1. Notice that this point is in the ridge A. Here transitions in both mantle layers are non-zero but have opposite sign and cancel each other. So, the whole effect is due to MSW resonance enhancement in core.

For large 1-3 mixing, e.g. $\sin^2 2\theta_{13} = 0.125$, there is substantial interplay of the core and mantle oscillation effects (see figure 6). For $\Theta_\nu \sim 0$, we find $\phi_1 \sim \phi_2 < \pi$; contributions from two mantle layers interfere constructively and the total mantle contribution is comparable with the core contribution (the later is resonantly enhanced).

The parametric ridges differ by the oscillation phase acquired in the core, ϕ_2.

Ridge A. The phase in the core $\phi_2 \lesssim \pi$. This ridge lies in between the core resonance (at $\Theta_\nu \sim 0^\circ$) and the mantle resonance regions. At the border between the core and the mantle domains of the oscillogram, $\Theta_\nu = 33.1^\circ$, this ridge merges with the MSW resonance peak in the mantle.

As we mentioned above, for $\Theta_\nu < 10^\circ$ and $E_\nu \sim 3\,\mathrm{GeV}$ the phase in the core $\phi_2 < \pi/2$, the mantle effect is small and two mantle layer contributions cancel each other. So, here we deal with resonance enhancement of oscillations in core. With increase of E_ν and Θ_ν along the ridge both phases ϕ_1 and ϕ_2 decrease. The core and two mantle contributions add constructively leading to large probability. For example, for the point A_3 (Fig 5) $\pi_1 \approx \pi_2 \approx \pi/3$ and maximal probability build up by three comparable contributions. The graphical representation of this evolution is shown figure 7c. For the core part we show in some panels two precession cones, corresponding to the beginning and the end of the core section. The difference of these two cones reflects the effects of the non-constant density distribution.

For large 1-3 mixing $\sin^2 2\theta_{13} \geq 0.075$, the region of maximal transition shifts to the mantle domain. Furthermore, the saddle point appear between the MSW resonance and the parametric resonance regions. In the saddle point A_1 (figure 6) the phases in the core and the mantle $\phi_1 \approx \phi_2 \approx \pi/2$, correspond to maximal oscillatory factors. However the contributions from the two mantle layers have opposite sign and cancel each other. The corresponding graphical representation is shown in figure 7f.

With increase of Θ_ν the phases ϕ_1 and ϕ_2 decrease and cancellation becomes weaker.

In the ridge A for small 1-3 mixing the lines of the phase and amplitude conditions almost coincide that ensures stability of enhancement in large area.

Ridge B. This ridge is situated at $E_\nu \geq 5\,\mathrm{GeV}$. For the smallest energies in the ridge and $\Theta_\nu \sim 0$ the half-phase in the core $\phi_2 \sim (1.2 - 1.3)\pi$, so that oscillations in the core give substantial contribution effect (see figures 5 and 6). In the range $E_\nu = (5-6)\,\mathrm{GeV}$ the parametric enhancement of oscillations with significant interplay of the core and mantle oscillation effects is realized. In figure 7d we show graphical representation for the point B_2 (figure 6).

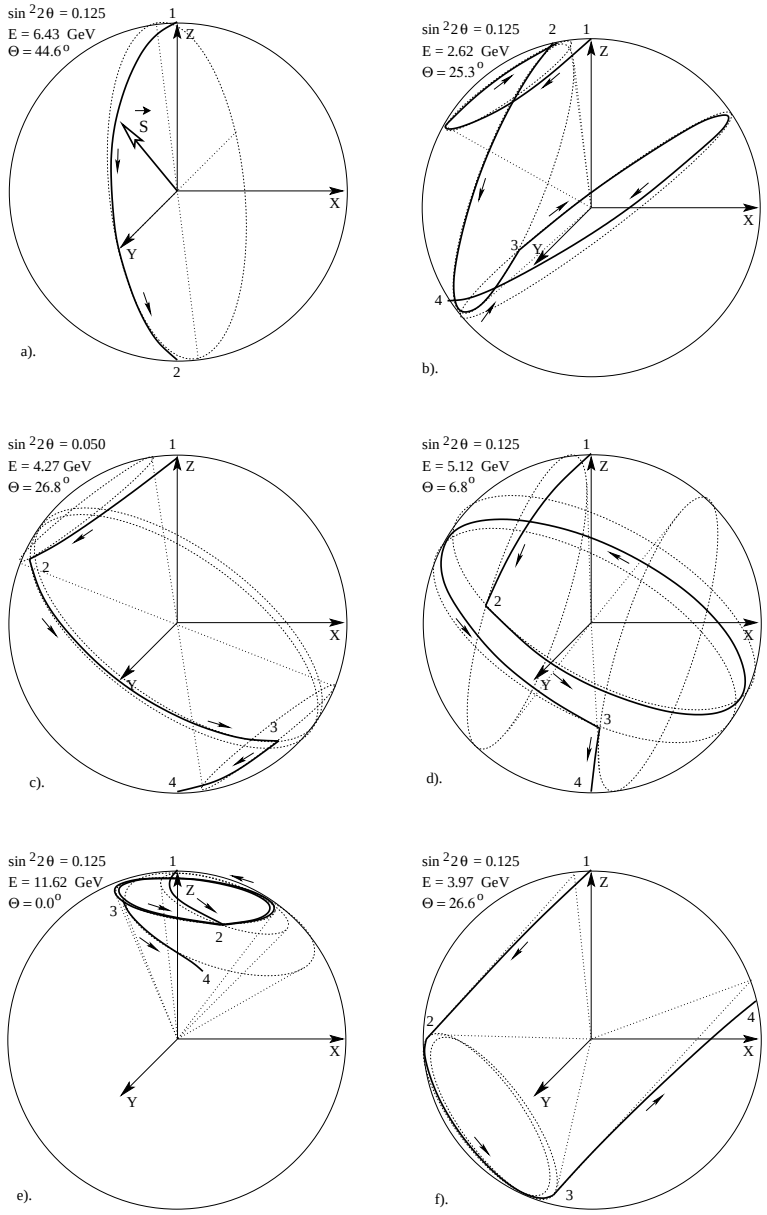

Figure 7: Graphical representation of neutrino evolution in the Earth. Shown are the trajectories of the neutrino vector $\vec{s}$ in the (X, Y, Z) space (solid lines), for different values of θ_{13} and different points in the oscillograms. The different panels correspond to a) the MSW peak in mantle; b) the point Z_2 in figure 6; c) the point A_3 in figure 5; d) the point B_2 in figure 6; e) the point C_1 in figure 6; f) near saddle point A_1 in figure 6. We also show the precession cones (dotted lines) in the mantle and core points close to the border between the mantle and core. Sections 1-2, 2-3 and 3-4 indicate evolution in the first mantle layer, the core and the second mantle layer correspondingly.

Ridge C. The ridge is located at $E_\nu > 11\,\mathrm{GeV}$ in the matter dominated region where mixing and consequently oscillation depth are suppressed. For $\Theta_\nu \sim 0$ the half-phase in the core equals $\phi_2 \sim 1.8\pi$. Here main contribution to probability is due to oscillations in mantle

JHEP05(2007)077

whereas the core gives small (negative) contribution. We show graphical representation of evolution that corresponds to the point C_1 in figure 7e.

Notice that qualitative features of the high energy part of ridge B and ridge C do not depend on θ_{13} since both are in the θ_{13} factorization region where $P_A \propto \sin^2 2\theta_{13}$ (see section 5.1).

4. Approximate analytic description of neutrino oscillations in the Earth

In this section we develop an approximate analytic approach to 2-flavor neutrino oscillations in the Earth. To this end, we employ a perturbation theory in the deviation of the density profile from that represented by layers of constant densities. This approach has been first developed in ref. [32] for the description of the solar neutrino oscillations in the earth. Here we apply it to the study of atmospheric neutrinos. The approximation turns out to work extremely well in spite of the fact that the variations of the neutrino potential inside the Earth layers can be large $|\Delta V|/\bar{V} \sim 0.3$. The high accuracy of our approach is related to the symmetry of the density profile of the Earth.

4.1 Perturbation theory in ΔV

Let us first consider the case of one layer of relatively weakly varying density and represent the matter-induced potential of neutrinos $V(x)$ along a given trajectory as the sum of a constant term $\bar{V}$ and a perturbation $\Delta V(x)$:

$$V(x) = \bar{V} + \Delta V(x)\,. \tag{4.1}$$

Correspondingly, the Hamiltonian of the system can be written as the sum of two terms:

$$H(x) = \bar{H} + \Delta H(x)\,, \tag{4.2}$$

where

$$\bar{H} \equiv \bar{\omega} \begin{pmatrix} -\cos 2\bar{\theta} & \sin 2\bar{\theta} \\ \sin 2\bar{\theta} & \cos 2\bar{\theta} \end{pmatrix}, \qquad \Delta H \equiv \frac{\Delta V(x)}{2} \begin{pmatrix} 1 & 0 \\ 0 & -1 \end{pmatrix}. \tag{4.3}$$

Here $\bar{\theta} = \theta_m(\bar{V})$ is the mixing angle in matter and $\bar{\omega} = \omega(\bar{V})$ is half of the energy splitting (half-frequency) in matter, both with the average potential $\bar{V}$. Throughout this section we will denote by $\bar{S}(x)$ the evolution matrix of the system for the constant density case $H(x) = \bar{H}$. The explicit expression for $\bar{S}(x)$ is given by eq. (2.21) with $\theta_m = \bar{\theta}$.

For matter of varying density, we seek the solution of the evolution equation (2.3) in the form

$$S(x) = \bar{S}(x) + \Delta S(x), \qquad \Delta S(x) = -i\,\bar{S}(x)\,K_1(x)\,, \tag{4.4}$$

where $K_1(x)$ satisfies $|K_1(x)_{ab}| \ll 1$. Inserting eq. (4.4) into eq. (2.3), we find the following equation for $K_1(x)$ to the first order in $\Delta H(x)$ and $K_1(x)$:

$$\frac{dK_1(x)}{dx} = \bar{S}^\dagger(x)\,\Delta H(x)\,\bar{S}(x) = \frac{\Delta V(x)}{2} \left\{ -\cos 2\bar{\theta} \begin{pmatrix} -\cos 2\bar{\theta} & \sin 2\bar{\theta} \\ \sin 2\bar{\theta} & \cos 2\bar{\theta} \end{pmatrix} \right.$$
$$\left. + \sin 2\bar{\theta} \begin{pmatrix} \sin 2\bar{\theta} & \cos 2\bar{\theta} \\ \cos 2\bar{\theta} & -\sin 2\bar{\theta} \end{pmatrix} \cos 2\phi(x) + \sin 2\bar{\theta} \begin{pmatrix} 0 & -i \\ i & 0 \end{pmatrix} \sin 2\phi(x) \right\}. \tag{4.5}$$

The first term does not contribute to $S \equiv S(L)$ since $\langle \Delta V \rangle \equiv \int \Delta V(x) dx = 0$, and eq. (4.5) can be immediately integrated:

$$K_1(L) = \frac{1}{2} \sin 2\bar{\theta} \left\{ \begin{pmatrix} \sin 2\bar{\theta} & \cos 2\bar{\theta} \\ \cos 2\bar{\theta} & -\sin 2\bar{\theta} \end{pmatrix} \int_0^L \Delta V(x) \, \cos 2\phi(x) \, dx \right. \\ \left. + \begin{pmatrix} 0 & -i \\ i & 0 \end{pmatrix} \int_0^L \Delta V(x) \, \sin 2\phi(x) \, dx \right\} . \quad (4.6)$$

It is convenient to introduce the new variable $z = x - L/2$, which measures the distance from the midpoint of the neutrino trajectory. Then from (4.6) we obtain

$$\Delta S \equiv \Delta S(L) = -i \, \sin 2\bar{\theta} \left\{ \begin{pmatrix} \sin 2\bar{\theta} & \cos 2\bar{\theta} \\ \cos 2\bar{\theta} & -\sin 2\bar{\theta} \end{pmatrix} \Delta I + \begin{pmatrix} 0 & -i \\ i & 0 \end{pmatrix} \Delta J \right\} , \quad (4.7)$$

where

$$\Delta I \equiv \frac{1}{2} \int_{-L/2}^{L/2} \Delta V(z) \, \cos(2\bar{\omega} z) \, dz \, , \qquad \Delta J \equiv \frac{1}{2} \int_{-L/2}^{L/2} \Delta V(z) \, \sin(2\bar{\omega} z) \, dz \, . \quad (4.8)$$

In these integrals, $\Delta V(z) \equiv \Delta V(x(z))$ and $x(z) = z - L/2$. Obviously, ΔJ vanishes if the perturbation $\Delta V(z)$ is symmetric with respect to the midpoint of the trajectory. Analogously, ΔI vanishes if $\Delta V(z)$ is antisymmetric. The expression for S defined in eq. (4.4) with ΔS given in eqs. (4.7) and (4.8) is equivalent to eqs. (13–16) obtained in ref. [32] in the context of solar neutrino oscillations.

Let us now consider the issue of the unitarity of the obtained evolution matrix that can be important for numerical calculations. Since $\bar{S} \equiv \bar{S}(L)$ is unitary, we have

$$S^\dagger S = I + \Delta S^\dagger \bar{S} + \bar{S}^\dagger \Delta S + \Delta S^\dagger \Delta S. \quad (4.9)$$

The second and third terms on the r.h.s. of this equality cancel each other thus ensuring the unitarity of S at the first order in ΔS. In order to prove this it is convenient to parametrize the evolution matrix $\bar{S}$ and the perturbation ΔS (4.7) as in eq. (3.11):

$$Y = \cos\phi \, , \qquad \mathbf{X} = \sin\phi \left(\sin 2\bar{\theta}, \; 0, \; -\cos 2\bar{\theta} \right) , \quad (4.10)$$

$$\Delta Y = 0, \qquad \Delta \mathbf{X} = \varepsilon \left(\cos 2\bar{\theta} \, \cos\xi, \; \sin\xi, \; \sin 2\bar{\theta} \, \cos\xi \right) , \quad (4.11)$$

where $\phi \equiv \phi(L)$ and we have introduced

$$\varepsilon = \sin 2\bar{\theta} \, \sqrt{\Delta I^2 + \Delta J^2} \, , \qquad \xi = \arg(\Delta I + i \, \Delta J) \, . \quad (4.12)$$

It is easy to see that $\Delta S^\dagger \bar{S} + \bar{S}^\dagger \Delta S = Y \, \Delta Y + \mathbf{X} \cdot \Delta \mathbf{X} = 0$. The last term in eq. (4.9), $\Delta S^\dagger \Delta S$, violates the unitarity condition, however it is of order ε^2 and therefore it does not break consistency of our approximation. However, for practical purposes it would be useful to have an expression for S which is *exactly* unitary regardless of the size of the

perturbation, even if for large perturbations the formalism is no longer accurate. In order to do this, we first rewrite eq. (4.7) as follows:

$$\Delta S = \varepsilon\, S' \,, \qquad S' = -i \left\{ \begin{pmatrix} \sin 2\bar{\theta} & \cos 2\bar{\theta} \\ \cos 2\bar{\theta} & -\sin 2\bar{\theta} \end{pmatrix} \cos\xi + \begin{pmatrix} 0 & -i \\ i & 0 \end{pmatrix} \sin\xi \right\} , \tag{4.13}$$

and then we perform the following replacement in the expression for S:

$$S = \bar{S} + \varepsilon\, S' \quad \longrightarrow \quad S = \cos\varepsilon\, \bar{S} + \sin\varepsilon\, S' \,. \tag{4.14}$$

Note that both S' and $\bar{S}$ are unitary matrices, and that due to their specific form the combination on the right-hand-side of eq. (4.14) is exactly unitary. In our computations we use the exactly unitary matrix (4.14).

4.2 Application: mantle-only crossing trajectories

We shall now use the formalism of the previous subsection to derive an explicit formula for the transition probability for mantle-only crossing neutrino trajectories. Since the density profile is symmetric with respect to the midpoint of the trajectory, the term ΔJ is absent. From eqs. (2.21), (4.7) and (4.14) we immediately get

$$P_A = \left[\cos\varepsilon\, \sin 2\bar{\theta}\, \sin\phi + \sin\varepsilon\, \cos 2\bar{\theta}\right]^2 \approx \sin^2 2\bar{\theta}\, \left[\sin\phi + \Delta I\, \cos 2\bar{\theta}\right]^2 , \tag{4.15}$$

where $\varepsilon \equiv \sin 2\bar{\theta}\, \Delta I$ and $\phi \equiv \phi(L) = \bar{\omega} L$. Here the first term in the square brackets describes oscillations in constant density matter with average potential $\bar{V}_1$. In order to obtain an explicit formula for ΔI, we approximate the matter density profile along the neutrino trajectory by a parabola:

$$\Delta V(z) \approx V_1'' \left[\left(\frac{z}{L}\right)^2 - \frac{1}{12} \right] . \tag{4.16}$$

The average value $\bar{V}_1$ and the coefficient V_1'' depend only on the nadir angle Θ_ν, and are shown in figure 8. Inserting the expression for $\Delta V(z)$ into eq. (4.8) and integrating by parts, we obtain

$$\Delta I = \frac{V_1'' L}{12} f(\phi), \qquad f(\phi) \equiv \frac{3\phi\cos\phi + (\phi^2 - 3)\sin\phi}{\phi^3} \,. \tag{4.17}$$

The function $f(\phi)$ has the following features: for $\phi \to 0$ (outer trajectories), one has $f(\phi) \to -\phi^2/15$; for $\phi = \pi/2$ which corresponds to the maximum transition probability for a given mixing angle in matter, $f(\phi) \approx -0.13$; the function $|f(\phi)|$ reaches its maximum, $f(\phi) \approx -0.31$, at $\phi \simeq 1.07\pi$. The function $f(\phi)$ changes its sign at $\phi \sim 1.8\pi$, and for large ϕ it behaves as $f(\phi) \sim \sin\phi/\phi$.

From eqs. (4.15) and (4.17) it follows that:

- in the zeroth approximation, the transition probability is given by the standard oscillation formula for matter of constant density, with the oscillation amplitude determined by the mixing angle $\bar{\theta} = \theta_m(\bar{V}_1)$ and the phase $\phi = \omega(\bar{V}_1)L$;

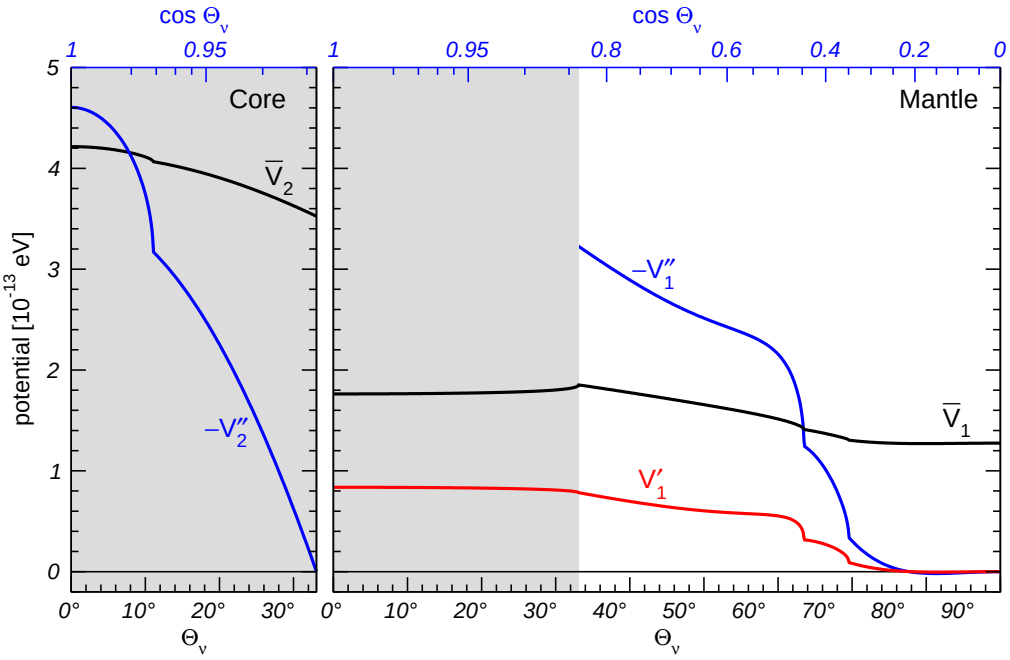

Figure 8: Dependence of the average potentials ($\bar{V}_1$, $\bar{V}_2$) (black) as well as the coefficients V_1' (red) and ($-V_1''$, $-V_2''$) (blue) on the nadir angle Θ_ν.

- the lowest-order correction to P_A vanishes at the MSW resonance, i.e. along the curve $E_R(\Theta_\nu)$. The correction changes its sign at the resonance, being positive below it ($E_\nu < E_R(\Theta_\nu)$) and negative above it;
- the largest corrections correspond to the trajectories with $\Theta_\nu \sim 37°$ (i.e. passing close to the core) and the phase $\phi \sim \pi$. Indeed, $f(\phi)$, $|V_1''|$ and L are all maximal for the deepest mantle trajectories

4.3 Application: core-crossing trajectories

For trajectories crossing the Earth's core, the evolution matrix can be factorized as

$$S = S_1^T \, S_2 \, S_1 \,, \tag{4.18}$$

where the subscripts '1' and '2' refer to the mantle (one layer) and core. S_1 and S_2 can be calculated using the formalism described in the previous sections. Since the core density profile is symmetric, the corresponding integral ΔJ_2 vanishes, whereas ΔI_2 can be calculated in full analogy with the derivation of ΔI in section 4.2. In particular, we can approximate the core density profile by a parabola and obtain for ΔI_2 an expression which is completely analogous to that in eq. (4.17): $\Delta I_2 = \Delta I(\phi_2, V_2'' L_2)$. Here $\phi_2 \equiv \bar{\omega}_2 L_2$ is the phase acquired in the core layer. The expression for S_2 is therefore

$$S_2 = \cos\varepsilon_2 \, \bar{S}_2 - i \, \sin\varepsilon_2 \begin{pmatrix} \sin 2\bar{\theta}_2 & \cos 2\bar{\theta}_2 \\ \cos 2\bar{\theta}_2 & -\sin 2\bar{\theta}_2 \end{pmatrix}, \qquad \varepsilon_2 = \sin 2\bar{\theta}_2 \, \Delta I_2 \,. \tag{4.19}$$

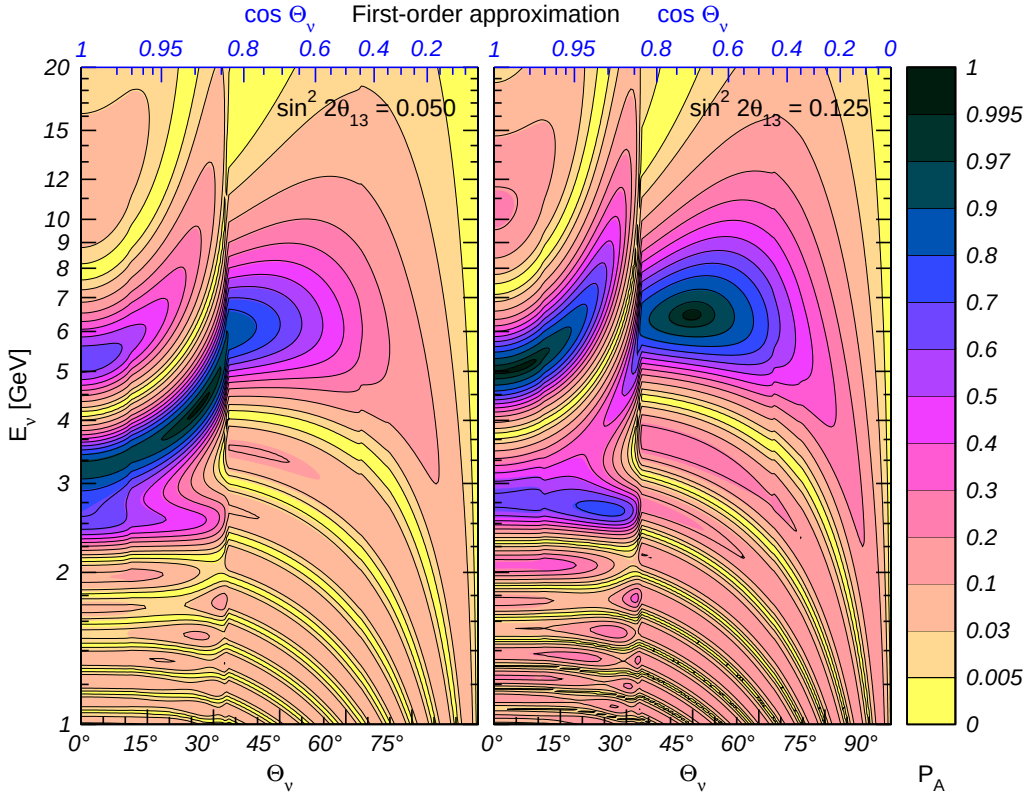

Figure 9: Contour plot of the probability P_A for the PREM density profile (colored regions; grayscale on black-and-white printouts) and for our analytic approximation including first-order corrections (black curves).

For the neutrino trajectories that cross the Earth's core, it is convenient to approximate the density profile within each mantle layer by a linear function of the coordinate:

$$V_1(z) = \bar{V}_1 + \Delta V_1(z), \qquad \Delta V_1(z) \approx V_1' \frac{z}{L_1}, \tag{4.20}$$

where L_1 is the length of one mantle layer. The advantage of this parametrization is that $\Delta V_1(z)$ is an antisymmetric function of z, and therefore ΔI_1 vanishes. For ΔJ_1 we obtain from eq. (4.8):

$$\Delta J_1 = V_1' L_1 \, \frac{\sin\phi_1 - \phi_1 \cos\phi_1}{4\phi_1^2} \tag{4.21}$$

where $\phi_1 \equiv \bar{\omega}_1 L_1$ is the phase acquired in each mantle layer. Then S_1 is given by

$$S_1 = \cos\varepsilon_1 \, \bar{S}_1 + \sin\varepsilon_1 \begin{pmatrix} 0 & -1 \\ 1 & 0 \end{pmatrix}, \qquad \varepsilon_1 = \sin 2\bar{\theta}_1 \, \Delta J_1 \, . \tag{4.22}$$

At first-order in ε_1:

$$S_1 \approx \begin{pmatrix} \cos\phi_1 + i\cos 2\bar{\theta}_1 \, \sin\phi_1 & \sin 2\bar{\theta}_1 \, (-i\sin\phi_1 - \Delta J_1) \\ \sin 2\bar{\theta}_1 \, (-i\sin\phi_1 + \Delta J_1) & \cos\phi_1 - i\cos 2\bar{\theta}_1 \, \sin\phi_1 \end{pmatrix}. \tag{4.23}$$

JHEP05(2007)077

In figure 8 we show the dependence of ($\bar{V}_1$, V_1') and ($\bar{V}_2$, V_2'') on the nadir angle Θ_ν. With these functions, one can find from eqs. (4.17) and eqs. (4.21) the quantities ΔI_2 and ΔJ_1 and then from eqs. (4.19) and (4.22) the evolution matrices S_1 and S_2. Substituting the results into eq. (4.18), one obtains the evolution matrix for the whole trajectory.

In the limit $|\Delta J_1| \ll |\sin\phi_1|$ eq. (4.23) can be rewritten as

$$S_1 = D_1\,\bar{S}_1\,D_1^*\,, \qquad D_1 \equiv \begin{pmatrix} e^{-i\tau_1/2} & 0 \\ 0 & e^{+i\tau_1/2} \end{pmatrix}\,, \qquad \tau_1 = \arcsin\left(\frac{\Delta J_1}{\sin\phi_1}\right)\,, \tag{4.24}$$

and since ΔJ_1 is real, D_1 is a pure phase matrix. In this limit the total evolution matrix eq. (4.18) takes the form

$$S = \bar{S}_1\,D_1\,S_2\,D_1\,\bar{S}_1 \tag{4.25}$$

where we have omitted the two outer matrices D_1^* are irrelevant for the calculation of $P_A = |S_{12}|^2$. The two matrices D_1 in eq. (4.25) can be combined with S_2 to construct an effective core matrix, which takes into account all the first-order corrections (both in the core and in the mantle):

$$S \equiv \bar{S}_1\,S_2'\,\bar{S}_1\,, \qquad S_2' \equiv D_1\,S_2\,D_1\,. \tag{4.26}$$

An advantage of this approach is that both $\bar{S}_1$ and S_2' are *symmetric* matrices, so that all the results derived previously in the constant-density approximation can be improved to take into account the first-order corrections by simply replacing $\bar{S}_2 \to S_2'$. The asymmetry of the mantle profile is effectively resolved.

In figure 9 we compare the P_A oscillograms obtained by numerical calculations for the PREM matter profile with those obtained using eqs. (4.18), (4.19) and (4.22). As can be seen from this figure the degree of accuracy increases drastically once the corrections described here are included.

An advantage of the described approximate analytic approach is that the coefficients $\bar{V}$ and V_1'' depend solely on the nadir angle of the neutrino trajectory Θ_ν. In particular, they do not depend on neutrino energy and on the values of Δm^2 and θ.

5. Dependence of oscillograms on 1-3 mixing, density profile and flavor channel

5.1 Dependence of oscillograms on 1-3 mixing

As can be seen in figure 1, with increasing $\sin^2 2\theta_{13}$ the oscillation probability increases everywhere in the (E_ν, Θ_ν) plane. The evolution of the oscillation pattern appears as a "flow" of higher probability along nearly fixed curves towards larger values of Θ_ν: The flow is along the curves of the phase condition (3.24) for the mantle trajectories, and along the curves of the collinearity condition for the core-crossing trajectories. These lines of flow move only weakly with θ_{13}.

The region of sizable oscillation probability, $P_A \geq 1/2$, appears first for $\sin^2 2\theta_{13} \approx 0.009$, at $\Theta_\nu = 0^\circ$ and $E_\nu = 2.8\,\mathrm{GeV}$. It is located on the parametric ridge A. This large

probability is due to the parametric enhancement of the oscillations. The nature of the increase of the oscillation probability with increasing θ_{13} is different in different regions of the parameter space. Analytic expressions for various structures in the oscillograms, derived in section 2.3, allow one to understand this evolution. Two features determine the dependence of the oscillograms on the 1-3 mixing:

- factorization of the θ_{13} dependent factors in the probability, and
- dependence of the amplitude and phase conditions on 1-3 mixing.

Let us consider first the regions outside the resonances: $E_\nu > E_R + \Delta E_R^{\max}$, and $E_\nu < E_R - \Delta E_R^{\max}$. Here $\Delta E_R^{\max} = E_R \tan 2\theta_{13}^{\max}$ and $\tan 2\theta_{13}^{\max} \sim (0.1-0.2)$ corresponds to the maximal allowed values of 1-3 mixing. In practice, for the mantle-crossing trajectories these are the regions with $E_\nu < 5\,\mathrm{GeV}$ and $E_\nu > 8\,\mathrm{GeV}$. In these regions, the mixing parameter in matter can be approximated by

$$\sin^2 2\theta_m \approx \frac{\sin^2 2\theta_{13}}{\left|1 - \frac{2VE_\nu}{\Delta m^2}\right|^2}\,. \tag{5.1}$$

Moreover, the half-phase

$$\phi \approx \frac{\Delta m^2}{4E_\nu}\left|1 - \frac{2VE_\nu}{\Delta m^2}\right| L \tag{5.2}$$

does not depend on 1-3 mixing. So, for the mantle domain trajectories the lines of constant phase that determine the lines of flow do not depend on 1-3 mixing. As follows from (5.1) and (5.2), the oscillation probability for one layer (mantle) factorizes:

$$P_A \approx \sin^2 2\theta_{13} \sin^2\phi \frac{1}{|1 - 2VE_\nu/\Delta m^2|^2}. \tag{5.3}$$

Therefore, the probability increases uniformly in the whole this area and the lines of zero and maximum transition probability do not move. For the core crossing trajectories similar analysis holds for $E_\nu < 2\,\mathrm{GeV}$.

Let us first consider the parametric resonance condition (3.13) that determines approximately the lines of "flow". Beyond the MSW resonance regions, the phases ϕ_i, and therefore c_i and s_i $(i = 1, 2)$, do not depend on the 1-3 mixing. The mixing angles in matter enter the condition through $\cos 2\theta_i$. Outside the resonance regions $\theta_i \approx \theta_{13} \ll 1$ or $\theta_i \approx \pi/2$ and therefore $\cos 2\theta_i \approx \pm 1$ weakly depend on 1-3 mixing. So, the condition (and therefore the lines of flow) shifts only weakly with change of θ_{13}.

Let us now consider the resonance regions $(2 < E_\nu < 12)\,\mathrm{GeV}$. Here dependence of the transition probability on $\sin^2 2\theta_{13}$ is non-linear. Not only the depth of the oscillations, but also the oscillation length in matter in each layer depends on $\sin^2 2\theta_{13}$ substantially, and the latter influences the interference effects. As a result, the transition probability changes with θ_{13} differently in different regions, and in addition the "lines of flow" shift.

One can make the following observations.

JHEP05(2007)077

- The MSW resonance peak in the mantle is determined by the condition (3.1). With increasing $\sin^2 2\theta_{13}$, the peak shifts to larger values of Θ_ν and to slightly larger energies. This can be readily understood. Indeed, the oscillation length at the resonance decreases with increasing θ_{13} as $l_m = l_\nu/\sin 2\theta_{13}$ and therefore the condition $\phi_1 = \pi/2$ is satisfied for shorter (more external) trajectories. For these trajectories the average density becomes smaller, so that the resonance energy increases: $E_R \propto 1/\bar{V}$. The width of the resonance peak at half height increases as $\tan 2\theta_{13}$ both in neutrino energy and in Θ_ν variables (see the discussion below eq. (3.1)). Using the resonance condition (3.1), we obtain from (3.4)

$$\tan 2\theta_{13} = \frac{\pi}{2\bar{V}(\Theta_\nu) R \cos\Theta_\nu} \equiv \frac{\pi}{d}\,, \tag{5.4}$$

  where d is the column density that corresponds to maximum of the transition probability. Eq. (5.4) gives an immediate relation between θ_{13} and the nadir angle of the neutrino trajectory on which the absolute maximum of the transition probability is realized. This can, in principle, be used for measuring θ_{13}: the method would simply consist in the determination of Θ_ν of the mantle-only crossing trajectory corresponding to the absolute maximum of the conversion probability $P_A = 1 - P_{ee}$.

- Core ridge slightly shifts with increase of θ_{13} to larger energies, especially at $\Theta_\nu \approx 0$.

- For ridge A, the region of sizable transition probability and the position of the maximum also move towards smaller $|\cos\Theta_\nu|$. With increasing θ_{13} the oscillation length decreases, especially in the resonance region. Therefore, the same phases in the core and mantle can be obtained for shorter trajectories in the core and therefore for larger Θ_ν.

- Ridge B evolves weaker with θ_{13}: the energy corresponding to the maximum of the transition probability stays rather close to that of the mantle MSW resonance, $E_\nu \approx (5-6)\,\mathrm{GeV}$. At higher energies the ridge is in the factorization region. With increase of θ_{13} at $\Theta_\nu \approx 0$ the ridge shifts to smaller E_ν.

- The situation for ridge C is similar to ridge B.

5.2 Dependence on the Earth's density profile

In different parts of the (E_ν, Θ_ν) plane the oscillation probabilities have different sensitivity to the modifications of matter density profile. The sensitivity is very weak (independently of the form of perturbation) in the following parts:

- $\Theta_\nu > 84^\circ$: here the length of the trajectory, and therefore the oscillation phase, are small, so that effect of "vacuum mimicking" [1, 5] takes place. To a good approximation matter does not affect the oscillation probabilities, irrespectively of whether or not the matter-induced potential V is small compared to the kinetic energy difference $\Delta m^2_{31}/2E_\nu$.

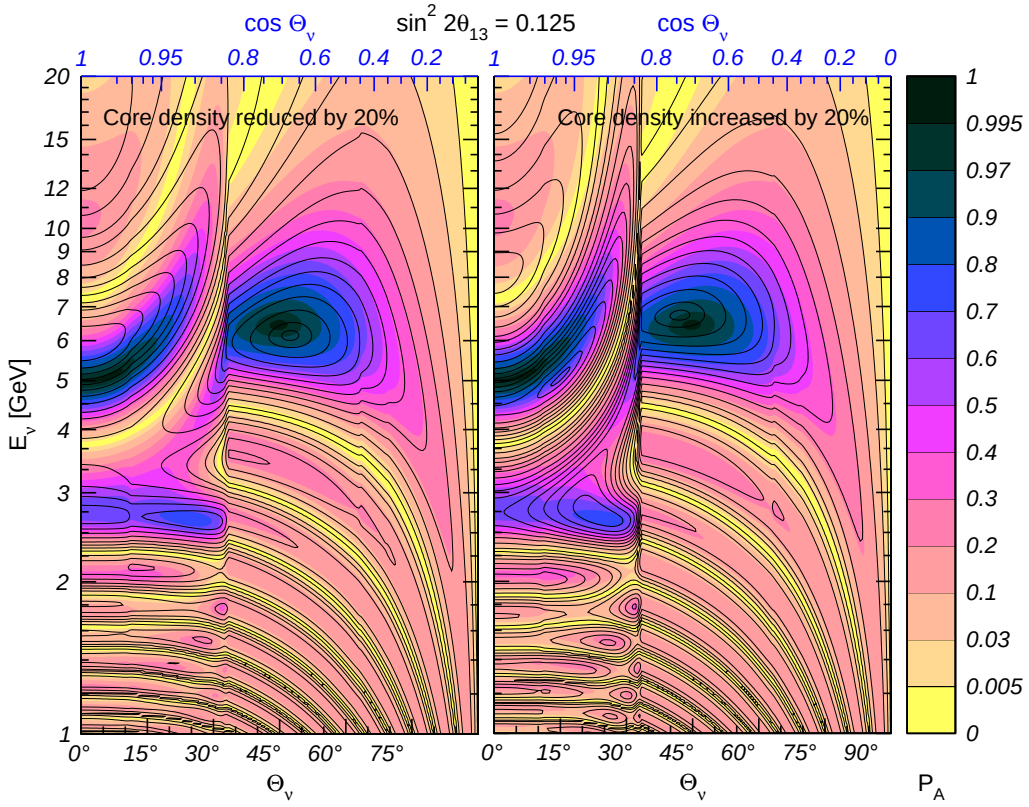

Figure 10: P_A oscillograms for the PREM density profile (colored regions) and for a 20% variations of the core/mantle density ratio. The total mass of the Earth is kept fixed.

- $E_\nu < 2\,\mathrm{GeV}$: here one has $V \ll \Delta m^2_{31}/2E_\nu$, and so matter effects on the oscillations driven by 1-3 mixing and splitting are small for all values of Θ_ν.

The region of high sensitivity to the density profile of the Earth is bounded by $E_\nu > (3-4)\,\mathrm{GeV}$ and $\Theta_\nu < 66°$. This is the region of energies close to and above the resonance energies (matter dominance) and of sufficiently long trajectories. The latter condition ensures an accumulation of the matter effects over long distances and therefore a sensitivity to large scale structures of the density profile. For the core-crossing trajectories the border of the sensitivity region is lower: $E_\nu \simeq 2\,\mathrm{GeV}$. Changes of the oscillograms in this region depend on the specific form of the modification of the matter density distribution.

For illustration, we consider here the effects of three different modifications of the Earth density profile: (1) replacing PREM profile by constant-density mantle and core layers, (2) modification of the core/mantle density ratio, and (3) changes of the position of the border between the mantle and the core.

(i) In figure 2 we show the results of the fixed constant-density layers approximation, characterized by the constant potentials V_1 and V_2 in the mantle and core. This profile can be considered as an extreme case of flattening of the mantle and core density distributions. For the mantle-only crossing trajectories there are two lines

JHEP05(2007)077

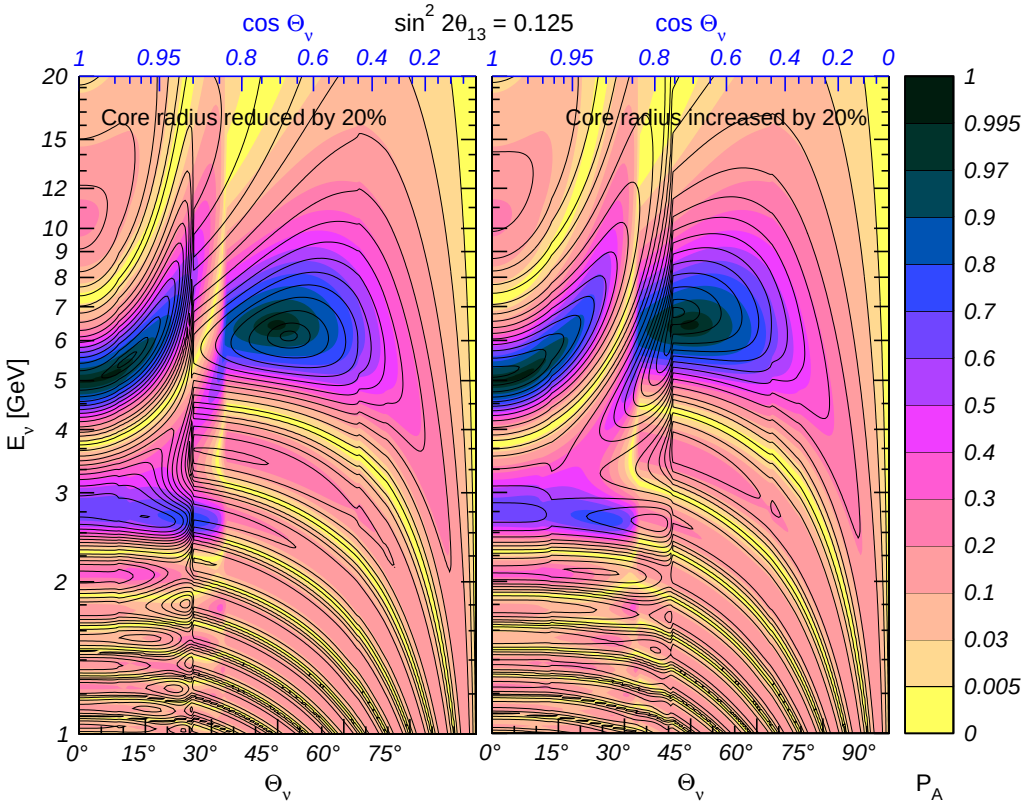

Figure 11: P_A oscillograms for the PREM density profile (colored regions) and for a 20% variations of the core radius. The total mass of the Earth is kept fixed.

in the oscillograms where the oscillation probabilities for the two profiles are equal: (i) $\Theta_\nu \approx 53^\circ$, which corresponds to the trajectory with $\bar{V}_{\rm PREM} = V_1$, and (ii) the resonance energy curve $E_\nu \simeq E_R(\Theta_\nu)$. Indeed, along the resonance curve the first-order correction to P_A due to the deviation of the density profile from the averaged constant one disappears (see the discussion in section 4.2).

For $\Theta_\nu < 53^\circ$ the oscillation pattern for the fixed constant-density profile is shifted to higher energies compared to that for the PREM profile. Furthermore, for $E_\nu > E_R(\Theta_\nu)$ one has $P_{\rm const} > P_{\rm PREM}$, whereas for lower energies, $E_\nu < E_R(\Theta_\nu)$, $P_{\rm const} < P_{\rm PREM}$, which essentially reflects the shift of the resonance peak when profile is changed. The shift of contours in the energy scale increases as Θ_ν decreases and reaches maximum for the deepest mantle trajectories.

For core crossing trajectories the size of changes is similar.

(ii) Figure 10 illustrates the effects of the increase (decrease) of the core density: $V_2(x) \to kV_2(x)$, where $k = const$. The shapes of the density profiles in the mantle and core are taken according to the PREM profile. The total mass of the Earth is unchanged and therefore the density of the mantle should be reduced (increased) correspondingly: $\Delta V_1/V_1 = -[(R/R_c)^3 - 1]^{-1}(\bar{V}_2/\bar{V}_1)\Delta V_2/V_2 \approx -0.3\Delta V_2/V_2$. The effects of the

increase and decrease of the core potential on the oscillogram are opposite and for definiteness we will consider the case of an increase of V_2. The strongest effect is for $\Theta_\nu < 60^\circ$ and above the resonance.

For core-crossing trajectories, an increase of the core density leads to a shift of the oscillatory pattern to larger Θ_ν and higher energies, and also results in an increase of probability. These features can be understood using the parametric resonance condition.

(iii) Figure 11 illustrates the effects of increase (decrease) of the core radius. Again, the requirement of keeping the total mass of the Earth fixed imposes a rescaling of the overall core and mantle densities. As in the previous case, this rescaling is what induces the most important effects on the oscillogram.

The sensitivity of the oscillation probabilities to the variations of the matter density distribution in the Earth can in principle be used for studying the Earth interior with neutrinos, i.e. to perform an oscillation tomography of the Earth [39]. Using the features described above one can work out the criteria for the selection of events that are sensitive to a given type of variations of the profile.

5.3 Probabilities for other oscillation channels

In figures 12 and 13 we show the oscillograms for the other channels. As follows from the discussion in section 2.2, in the approximation of zero 1-2 splitting ($\Delta m^2_{21} = 0$) all the probabilities that involve ν_e depend on the single probability P_A. This is related to the fact that ν_e is unchanged upon going from the flavor basis to the propagation one.

The probability $P_{ee} = 1 - P_A$ is just complementary to P_A with all the features inverted. $P_{e\mu}$ is just P_A scaled by the factor s^2_{23} (see the middle panel in figure 12). The maximal value of this transition probability is therefore s^2_{23}. Similarly, $P_{e\tau}$ is P_A scaled by the factor c^2_{23}.

The probabilities of transitions that do not involve ν_e have more complicated structure since now both the initial and the final states do not belong to the propagation basis and therefore some additional interference occurs. The survival probability $P_{\mu\mu}$ in eq. (2.16) can be written as

$$P_{\mu\mu} = P_{\rm vac} - s^4_{23} P_A + 2 s^2_{23} c^2_{23} \left({\rm Re}\, A_{33} - \cos 2\phi_{\rm vac} \right), \tag{5.5}$$

where $P_{\rm vac} = 1 - \sin^2 2\theta_{23} \sin^2 \phi_{\rm vac}$ is the usual 2-flavor vacuum oscillation probability and $\phi_{\rm vac} \equiv \Delta m^2_{31} L/4E_\nu$ is the vacuum oscillation phase. $P_{\rm vac}$ describes the oscillation effect in the absence on the 1-3 mixing. The other two terms in (5.5) describe the effects of the 1-3 mixing. We can use the approximate results of section 4 to estimate ${\rm Re}\, A_{33}$. Recall that in section 4 we used a symmetric Hamiltonian for 2ν system, which differs from the one introduced in section 2.1 by a term proportional to the unit matrix (2.19). The term ${\rm Re}\, A_{33}$ essentially reflects evolution of the 1-3 system with respect to the state $\tilde{\nu}_2$ and so the 3ν form of the Hamiltonian should be restored. According to eq. (2.19) the relation

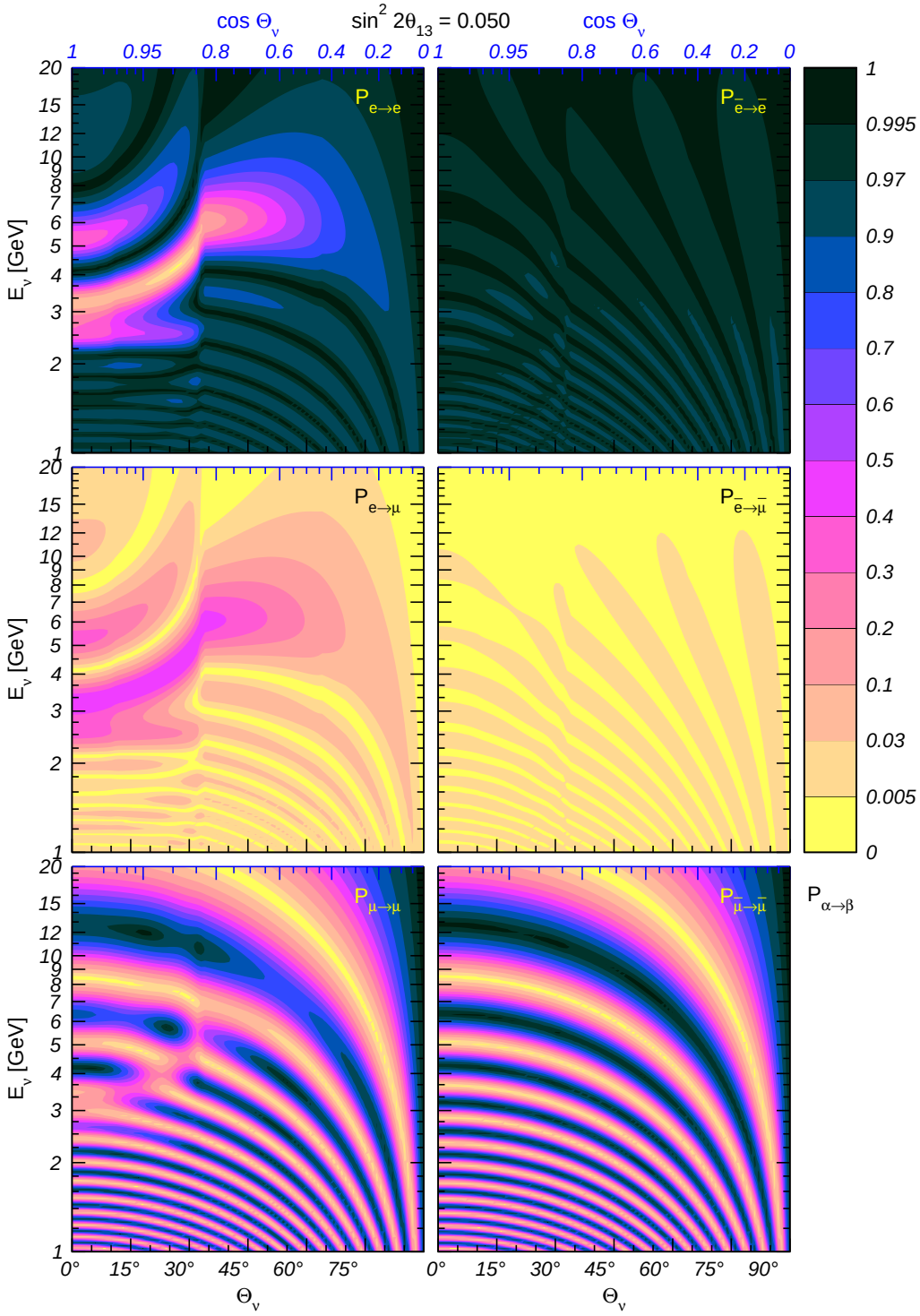

Figure 12: P_{ee}, $P_{e\mu}$ and $P_{\mu\mu}$ oscillograms, for neutrinos (left panels) and antineutrinos (right panels), $\sin^2 2\theta_{13} = 0.05$, $\sin^2 2\theta_{23} = 1$ and $\Delta m^2_{21} = 0$.

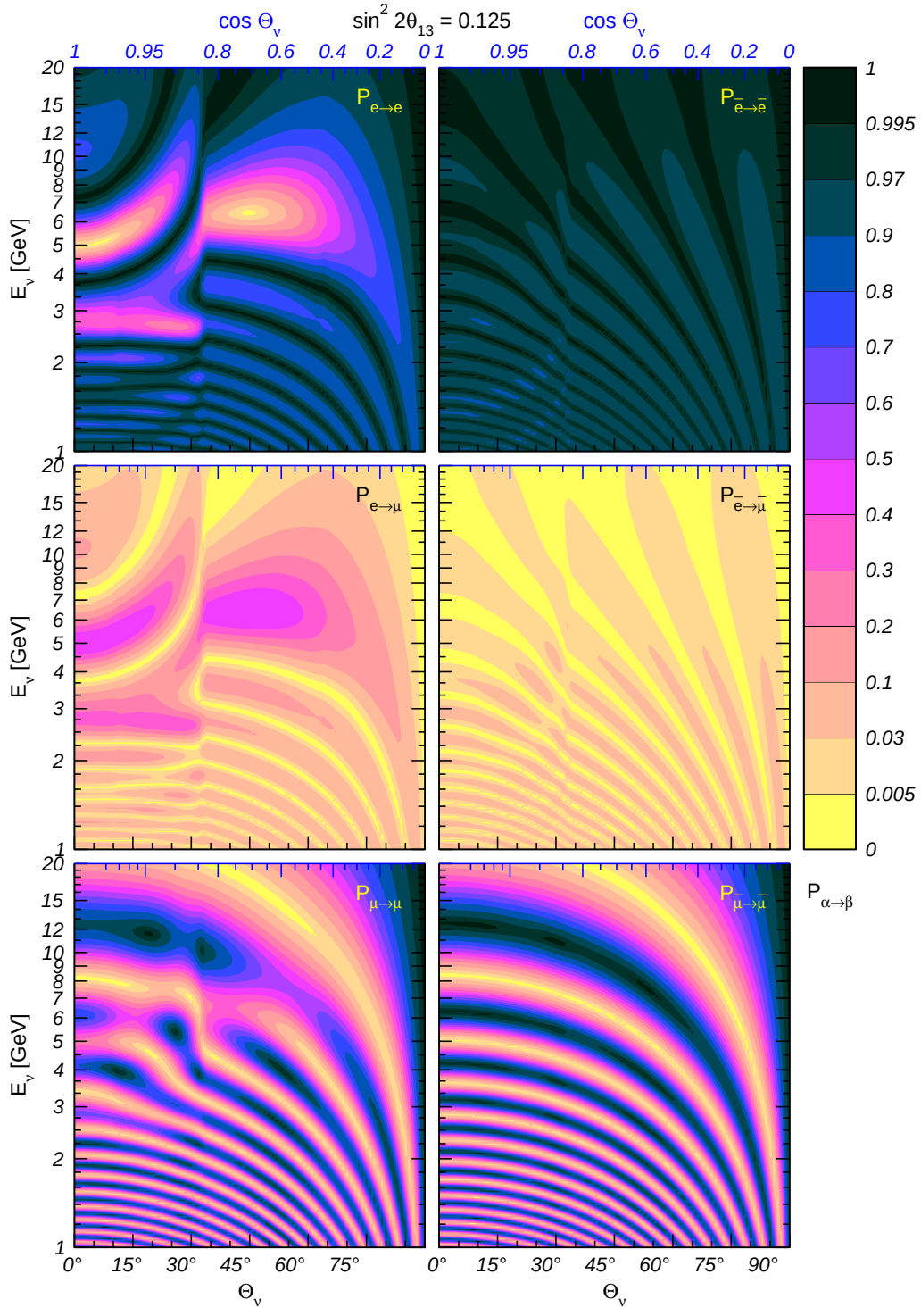

Figure 13: The same as in figure 12 but for $\sin^2 2\theta_{13} = 0.125$.

between the corresponding evolution matrices (up to the removed decoupled state) is

$$\tilde{S} = e^{-i\psi} S, \qquad \psi \equiv \int_0^L \left(\frac{\Delta m^2_{31}}{4E_\nu} + \frac{V}{2} \right) dx \,. \tag{5.6}$$

Then

$$A_{33} = e^{-i\psi}\, S_{22}\,, \tag{5.7}$$

where S_{22} is the 22 element of the matrix (2.21) with the correction given in (4.7).

Let us consider the mantle trajectories. Then from (5.7) we get explicitly

$$\mathrm{Re}\, A_{33} = \cos(\phi+\psi) + 2\sin^2\bar{\theta}_{13}\sin\psi[\sin\phi + 2\cos^2\bar{\theta}_{13}\Delta I]\,, \tag{5.8}$$

where the phase ϕ and the correction integral ΔI are defined in (2.21) and (4.8), respectively, and the angle $\bar{\theta}_{13}$ is the 1-3 mixing angle in matter calculated at the average value of the matter density. Then the survival probability $P_{\mu\mu}$ for the mantle-only crossing trajectory can be written as

$$P_{\mu\mu} = 1 - \sin^2 2\theta_{23}\sin^2\left(\frac{\phi+\psi}{2}\right) - s_{23}^4 P_A + \frac{1}{2}\sin^2 2\theta_{23}\sin\psi\left(2\sin^2\bar{\theta}_{13}\sin\phi + \sin^2 2\bar{\theta}_{13}\,\Delta I\right)\,. \tag{5.9}$$

Notice that the first two terms here correspond to 2-flavor vacuum probability with the modified phase. The probability can be rewritten as

$$P_{\mu\mu} = P_{\rm vac} + \Delta P \tag{5.10}$$

with

$$\Delta P = -s_{23}^4 P_A - 2s_{23}^2 c_{23}^2\big[\cos 2\phi_{\rm vac} - \cos(\phi+\psi) - 2\sin^2\bar{\theta}_{13}\sin\psi\sin\phi - \sin^2 2\bar{\theta}_{13}\sin\psi\,\Delta I\big]. \tag{5.11}$$

In the limit $s_{13}\to 0$ one has

$$\phi \approx \int_0^L \left(\frac{\Delta m^2}{4E_\nu} - \frac{V(x)}{2}\right) dx \tag{5.12}$$

which, together with (5.6), implies $\phi+\psi = 2\phi_{\rm vac}$.

These formulas can be used for the analysis of numerical results shown in figures 12 and 13. The first correction term in eq. (5.11) is negative, so that it reduces the survival probability. The strongest effect of this mixing occurs in the resonance region. For high energies the 1-3 mixing is suppressed and $P_{\mu\mu}$ is again described well by the vacuum oscillation formula. Notice that in some regions with zero $P_{\rm vac}$ the 1-3 mixing leads to the positive contribution which is due to the last term in (5.5) so that the lines of of zero probability are interrupted. Also there are no lines of maximal probability, as zero lines for P_A.

All the correction terms to $P_{\rm vac}$ are in general of the same order; therefore the modification of the vacuum probability is rather complex and not immediately related to $P_{e\mu}$. The corrections are in general large in the regions of the parameter space where $P_{e\mu}$ is large, i.e. in the resonance regions and in the places of the resonance peaks and parametric ridges of P_A. Instead of continuous lines of maximal probability, in the case of non-zero

JHEP05(2007)077

1-3 mixing one obtains saddle points and local maxima. In particular, the saddle point of the $P_{\mu\mu}$ probability appears in the mantle resonance region.

The structure of the transition probability $P_{\mu\tau}$ is similar to that of $P_{\mu\mu}$.

In the antineutrino channel, the 2-flavor probability $\bar{P}_2$ is suppressed by matter and the strongest transitions occur in the vacuum oscillation region. Some interference effects are seen for the core domain but no substantial parametric enhancement is realized.

6. Discussion and conclusions

1. We have worked out a detailed and comprehensive description of neutrino oscillations driven by non-zero 1-3 mixing inside the Earth. The description is given in terms of the oscillograms of the Earth: contours of constant oscillation probabilities in the (E_ν, Θ_ν) plane. In this first publication we have neglected the 1-2 mass splitting Δm^2_{21}, which is a good approximation for high neutrino energies, $E_\nu > 1 - 2\,\mathrm{GeV}$.

2. We found that the oscillograms have a regular structure with several generic features: (i) the MSW peak in the mantle domain of the oscillogram; (ii) the MSW peak (ridge) in the core domain, (iii) three parametric ridges in the core domain; (iv) regular oscillatory pattern at low energies that has different features in the core and in the mantle domains of the oscillograms. We presented a detailed description of these structures: their position in the (E_ν, Θ_ν) plane, their evolution with changing 1-3 mixing and their dependence on the density profile of the Earth.

The most interesting features of the oscillograms appear at relatively high energies, $E_\nu = (2 - 12)\,\mathrm{GeV}$, and $\Theta_\nu < 75^\circ$, i.e. in the resonance region. Notice that this region is not covered by the existing or forthcoming accelerator experiments, and on the other hand, statistics in the current atmospheric neutrino experiments is too low. All these experiments can only study very small effects on the "tails" of those interesting oscillation phenomena. Exploration of the resonance regions thus constitutes a significant experimental challenge for future experiments.

3. We studied the accuracy of the calculations based on the constant-density layers approximation to the Earth matter density profile. This approximation reproduces all the features of the oscillograms qualitatively well, though there are some quantitative differences and shifts of the structures in the (E_ν, Θ_ν) plane. The strongest deviations appear in the domain of deep mantle trajectories and high energies $(E_\nu > 6\,\mathrm{GeV})$.

4. We showed that a complete physics interpretation of the oscillograms can be given in terms of different realizations of just two conditions: (i) the amplitude (or resonance) condition and (ii) the phase condition. In the case of one layer of constant density these conditions are reduced to the MSW resonance condition and half-phase equality $\phi = \pi/2 + \pi k$. They determine the position of the absolute maxima of the transition probability. For three layers of constant densities the amplitude condition is reduced to the parametric resonance condition. This condition describes the position of the parametric ridges. The phase condition gives the position of the maximum along the ridge.

JHEP05(2007)077

We show that the parametric resonance condition formulated for two layers describes the extrema and the ridges in the three layers case. This is a consequence of the symmetry of the overall matter density profile. In the case of three layers, the amplitude and the phase conditions determine not only the absolute maxima of the transition probability (as in the one-layer case), but also its local maxima and saddle points.

5. We generalized the amplitude and phase conditions to the case of varying densities in each layer. The generalization is not unique. In this connection we introduced the generalized resonance condition and the collinearity condition. The two conditions coincide in the case of constant density layers with symmetric overall profiles but differ in the non-constant density case. We showed that both these generalized conditions describe the positions of various structures of the oscillograms, in particular, of the extrema, very accurately.

6. We derived approximate analytic formulas for the probabilities. For this we have developed a perturbation theory in deviations from the constant density $\Delta V/\bar{V}$. We showed that already the first order approximation in $\Delta V/\bar{V}$ reproduces the oscillograms for realistic (PREM) density profile of the Earth with a high precision. Again, the symmetry of the density profile plays the key role.

7. We studied the dependence of the oscillograms on θ_{13}. The changes of the oscillograms with increasing θ_{13} have a character of flow of high probabilities towards the regions of larger Θ_ν. The lines of flow shift only weakly with changing θ_{13}. We found that the transition probability P_A can be of the order 1 for $\sin^2 2\theta_{13}$ as small as 0.01. Therefore, even if the next generation of reactor and accelerator experiments fail to find non-zero 1-3 mixing, significant oscillation effects due to this mixing may still show up in atmospheric neutrino data. Those are expected in the region $E_\nu \sim 3 - 5\,\mathrm{GeV}$ and $\Theta_\nu \approx 0^\circ - 26^\circ$.

8. We studied the dependence of the oscillograms on the density profile of the Earth. We found the regions in the (E_ν, Θ_ν) plane where the sensitivity to various perturbations of the density profile is maximal, and we identified the corresponding effects. In particular, the dependence of the oscillograms on flattening of the density distributions inside the layers, on the changes of the overall densities of the core and mantle and on the position of the border between the mantle and the core has been quantified. This analysis can be used for discussions of the oscillation tomography of the Earth.

9. The oscillograms for different flavor channels as well as for neutrinos and antineutrinos have been constructed and their properties discussed.

Various applications of the results obtained in this paper will be presented in forthcoming publications.

Acknowledgments

We would like to thank T. Schwetz for useful discussions and E. Lisi and W. Winter for useful communications. EA was supported by the Wenner-Gren Foundation as an Axel

Wenner-Gren visiting professor at the Royal Institute of Technology. MM was supported by MCYT through the Ramón y Cajal program, by CiCYT through the project FPA2006-01105, and by the Comunidad Autónoma de Madrid through the project P-ESP-00346.

References

[1] L. Wolfenstein, *Neutrino oscillations in matter*, *Phys. Rev.* **D 17** (1978) 2369.

[2] S.P. Mikheev and A.Y. Smirnov, *Resonance enhancement of oscillations in matter and solar neutrino spectroscopy*, *Sov. J. Nucl. Phys.* **42** (1985) 913 [*Yad. Fiz.* **42** (1985) 1441].

[3] S.P. Mikheyev and A.Yu. Smirnov, *′86 massive neutrinos in astrophysics and in particle physics*, proceedings of the Sixth Moriond Workshop, edited by O. Fackler and J. Trân Thanh Vân, Editions Frontières, Gif-sur-Yvette (1986).

[4] E.D. Carlson, *Terrestrially enhanced neutrino oscillations*, *Phys. Rev.* **D 34** (1986) 1454;
A. Dar, A. Mann, Y. Melina and D. Zajfman, *Neutrino oscillations and the solar neutrino problem*, *Phys. Rev.* **D 35** (1987) 3607;
G. Auriemma, M. Felcini, P. Lipari and J.L. Stone, *Resonant oscillations of atmospheric neutrinos with an underground muon detector*, *Phys. Rev.* **D 37** (1988) 665;
A.J. Baltz and J. Weneser, *Effect of transmission through the Earth on neutrino oscillations*, *Phys. Rev.* **D 35** (1987) 528;
M. Cribier, W. Hampel, J. Rich and D. Vignaud, *Msw regeneration of solar electron-neutrino in the Earth*, *Phys. Lett.* **B 182** (1986) 89;
A. Nicolaidis, *Neutrinos for geophysics*, *Phys. Lett.* **B 200** (1988) 553;
P.I. Krastev and S.T. Petcov, *Resonance amplification and T violation effects in three neutrino oscillations in the Earth*, *Phys. Lett.* **B 205** (1988) 84;
J.M. LoSecco, *Experimental tests of the MSW effect*, *Phys. Rev.* **D 47** (1993) 2032;
J.M. Gelb, W.-k. Kwong and S.P. Rosen, *Searching for the MSW enhancement*, *Phys. Rev. Lett.* **78** (1997) 2296 [hep-ph/9612332].

[5] A. De Rujula, M.B. Gavela and P. Hernandez, *Neutrino oscillation physics with a neutrino factory*, *Nucl. Phys.* **B 547** (1999) 21 [hep-ph/9811390];
E.K. Akhmedov, *Matter effects in short-baseline neutrino oscillations*, *Phys. Lett.* **B 503** (2001) 133 [hep-ph/0011136];
O. Yasuda, *Vacuum mimicking phenomena in neutrino oscillations*, *Phys. Lett.* **B 516** (2001) 111 [hep-ph/0106232].

[6] J.T. Pantaleone, *Constraints on three neutrino mixing from atmospheric and reactor data*, *Phys. Rev.* **D 49** (1994) 2152 [hep-ph/9310363];
G.L. Fogli, E. Lisi, D. Montanino and G. Scioscia, *Three-flavor atmospheric neutrino anomaly*, *Phys. Rev.* **D 55** (1997) 4385 [hep-ph/9607251];
G.L. Fogli, E. Lisi and A. Marrone, *Upward-going muons and neutrino oscillations*, *Phys. Rev.* **D 57** (1998) 5893 [hep-ph/9708213];
O. Yasuda, *Three flavor neutrino oscillation analysis of the Kamiokande atmospheric neutrino data*, hep-ph/9706546; *Three flavor neutrino oscillation analysis of the SuperKamiokande atmospheric neutrino data*, *Phys. Rev.* **D 58** (1998) 091301 [hep-ph/9804400];
C. Giunti, C.W. Kim and J.D. Kim, *Atmospheric neutrino problem in maximally mixed three generations of neutrinos*, *Phys. Lett.* **B 352** (1995) 357 [hep-ph/9411219];

JHEP05(2007)077

P.F. Harrison, D.H. Perkins and W.G. Scott, *Threefold maximal lepton mixing and the solar and atmospheric neutrino deficits*, *Phys. Lett.* **B 349** (1995) 137; *Further evidence for threefold maximal lepton mixing and a hierarchical spectrum of neutrino mass-squared differences*, *Phys. Lett.* **B 396** (1997) 186 [hep-ph/9702243];
H. Fritzsch and Z.-Z. Xing, *Lepton mass hierarchy and neutrino oscillations*, *Phys. Lett.* **B 372** (1996) 265 [hep-ph/9509389];
C. Giunti, C.W. Kim and M. Monteno, *Atmospheric neutrino oscillations with three neutrinos and a mass hierarchy*, *Nucl. Phys.* **B 521** (1998) 3 [hep-ph/9709439];
R. Foot, R.R. Volkas and O. Yasuda, *Up-down atmospheric neutrino flux asymmetry predictions for various neutrino oscillation scenarios*, *Phys. Lett.* **B 421** (1998) 245 [hep-ph/9710403];
G.L. Fogli, E. Lisi, A. Marrone and D. Montanino, *Zenith distribution of atmospheric neutrino events and electron neutrino mixing*, *Phys. Lett.* **B 425** (1998) 341 [hep-ph/9711421].

[7] M. Freund, M. Lindner, S.T. Petcov and A. Romanino, *Testing matter effects in very long baseline neutrino oscillation experiments*, *Nucl. Phys.* **B 578** (2000) 27 [hep-ph/9912457].

[8] T. Ohlsson and H. Snellman, *Neutrino oscillations with three flavors in matter: applications to neutrinos traversing the Earth*, *Phys. Lett.* **B 474** (2000) 153 [hep-ph/9912295].

[9] I. Mocioiu and R. Shrock, *Matter effects on neutrino oscillations in long baseline experiments*, *Phys. Rev.* **D 62** (2000) 053017 [hep-ph/0002149];
M.C. Banuls, G. Barenboim and J. Bernabeu, *Medium effects for terrestrial and atmospheric neutrino oscillations*, *Phys. Lett.* **B 513** (2001) 391 [hep-ph/0102184].

[10] D. Indumathi and M.V.N. Murthy, *A question of hierarchy: matter effects with atmospheric neutrinos and anti-neutrinos*, *Phys. Rev.* **D 71** (2005) 013001 [hep-ph/0407336];
S. Palomares-Ruiz and S.T. Petcov, *Three-neutrino oscillations of atmospheric neutrinos, theta(13), neutrino mass hierarchy and iron magnetized detectors*, *Nucl. Phys.* **B 712** (2005) 392 [hep-ph/0406096].

[11] R. Gandhi, P. Ghoshal, S. Goswami, P. Mehta and S. Uma Sankar, *Earth matter effects at very long baselines and the neutrino mass hierarchy*, *Phys. Rev.* **D 73** (2006) 053001 [hep-ph/0411252].

[12] S.K. Agarwalla, S. Choubey, S. Goswami and A. Raychaudhuri, *Neutrino parameters from matter effects in p_{ee} at long baselines*, hep-ph/0611233.

[13] S.K. Agarwalla, S. Choubey and A. Raychaudhuri, *Neutrino mass hierarchy and theta(13) with a magic baseline beta-beam experiment*, *Nucl. Phys.* **B 771** (2007) 1 [hep-ph/0610333].

[14] M. Freund and T. Ohlsson, *Matter enhanced neutrino oscillations with a realistic Earth density profile*, *Mod. Phys. Lett.* **A 15** (2000) 867 [hep-ph/9909501].

[15] R. Gandhi, P. Ghoshal, S. Goswami, P. Mehta and S. Uma Sankar, *Large matter effects in $\nu_\mu \to \nu_\tau$ oscillations*, *Phys. Rev. Lett.* **94** (2005) 051801 [hep-ph/0408361].

[16] G.-L. Lin and Y. Umeda, *The matter effects to neutrino oscillations $\nu_\mu \to \nu_e$, ν_μ at very long baselines and the neutrino mixing angles theta(13) and theta(23)*, hep-ph/0505009.

[17] Q.Y. Liu and A.Y. Smirnov, *Neutrino mass spectrum with $\nu_\mu \to \nu_s$ oscillations of atmospheric neutrinos*, *Nucl. Phys.* **B 524** (1998) 505 [hep-ph/9712493]; *Parametric resonance in oscillations of atmospheric neutrinos?*, *Phys. Lett.* **B 440** (1998) 319 [hep-ph/9803415].

JHEP05(2007)077

[18] S.T. Petcov, *Diffractive-like (or parametric-resonance-like?) enhancement of the Earth (day-night) effect for solar neutrinos crossing the Earth core*, *Phys. Lett.* **B 434** (1998) 321 [hep-ph/9805262].

[19] E.K. Akhmedov, *Parametric resonance of neutrino oscillations and passage of solar and atmospheric neutrinos through the Earth*, *Nucl. Phys.* **B 538** (1999) 25 [hep-ph/9805272].

[20] E.K. Akhmedov, A. Dighe, P. Lipari and A.Y. Smirnov, *Atmospheric neutrinos at Super-Kamiokande and parametric resonance in neutrino oscillations*, *Nucl. Phys.* **B 542** (1999) 3 [hep-ph/9808270].

[21] M. Chizhov, M. Maris and S.T. Petcov, *On the oscillation length resonance in the transitions of solar and atmospheric neutrinos crossing the Earth core*, hep-ph/9810501.

[22] M.V. Chizhov and S.T. Petcov, *Enhancing mechanisms of neutrino transitions in a medium of nonperiodic constant-density layers and in the Earth*, *Phys. Rev.* **D 63** (2001) 073003 [hep-ph/9903424].

[23] E.K. Akhmedov and A.Y. Smirnov, *Comment on 'new conditions for a total neutrino conversion in a medium'*, *Phys. Rev. Lett.* **85** (2000) 3978 [hep-ph/9910433].

[24] V.K. Ermilova, V. A. Tsarev and V. A. Chechin, *Parametric resonance in neutrino oscillations*, *Kr. Soob. Fiz.* **5** (1986) 26, Short Notices of the Lebedev Institute.

[25] E.K. Akhmedov, *On neutrino oscillations in a nonhomogeneous medium*, *Sov. J. Nucl. Phys.* **47** (1988) 301 [*Yad. Fiz.* **47** (1988) 301].

[26] P.I. Krastev and A.Y. Smirnov, *Parametric effects in neutrino oscillations*, *Phys. Lett.* **B 226** (1989) 341.

[27] E.K. Akhmedov, M. Maltoni and A.Y. Smirnov, *Oscillations of high energy neutrinos in matter: precise formalism and parametric resonance*, *Phys. Rev. Lett.* **95** (2005) 211801 [hep-ph/0506064].

[28] P.M. Fishbane, *Neutrino oscillations in structured matter*, *Phys. Rev.* **D 62** (2000) 093009 [hep-ph/0004075].

[29] T. Ota and J. Sato, *Matter profile effect in neutrino factory*, *Phys. Rev.* **D 63** (2001) 093004 [hep-ph/0011234];
B. Jacobsson, T. Ohlsson, H. Snellman and W. Winter, *Effects of random matter density fluctuations on the neutrino oscillation transition probabilities in the Earth*, *Phys. Lett.* **B 532** (2002) 259 [hep-ph/0112138];
T. Ohlsson, *Effects and influences on neutrino oscillations due to a thin density layer perturbation added to a matter density profile*, *Phys. Lett.* **B 522** (2001) 280 [hep-ph/0109003];
P.-H. Gu, *Earth matter density uncertainty in atmospheric neutrino oscillations*, *Phys. Rev.* **D 72** (2005) 097301 [hep-ph/0511028];
E. Kozlovskaya, J. Peltoniemi and J. Sarkamo, *The density distribution in the Earth along the CERN-Pyhaesalmi baseline and its effect on neutrino oscillations*, hep-ph/0305042.

[30] T. Ohlsson and H. Snellman, *Three flavor neutrino oscillations in matter*, *J. Math. Phys.* **41** (2000) 2768 [hep-ph/9910546]; *Neutrino oscillations with three flavors in matter: applications to neutrinos traversing the Earth*, *Phys. Lett.* **B 474** (2000) 153 [hep-ph/9912295].

JHEP05(2007)077

[31] J. Bernabeu, S. Palomares-Ruiz, A. Perez and S.T. Petcov, *The Earth mantle-core effect in matter-induced asymmetries for atmospheric neutrino oscillations*, *Phys. Lett.* **B 531** (2002) 90 [hep-ph/0110071].

[32] E. Lisi and D. Montanino, *Earth regeneration effect in solar neutrino oscillations: an analytic approach*, *Phys. Rev.* **D 56** (1997) 1792 [hep-ph/9702343].

[33] A. Cervera et al., *Golden measurements at a neutrino factory*, *Nucl. Phys.* **B 579** (2000) 17 [Erratum *ibid.* **593** (2001) 731] [hep-ph/0002108];
M. Freund, *Analytic approximations for three neutrino oscillation parameters and probabilities in matter*, *Phys. Rev.* **D 64** (2001) 053003 [hep-ph/0103300];
E.K. Akhmedov, R. Johansson, M. Lindner, T. Ohlsson and T. Schwetz, *Series expansions for three-flavor neutrino oscillation probabilities in matter*, *JHEP* **04** (2004) 078 [hep-ph/0402175].

[34] B. Brahmachari, S. Choubey and P. Roy, *CP-violation and matter effect for a variable Earth density in very long baseline experiments*, *Nucl. Phys.* **B 671** (2003) 483 [hep-ph/0303078].

[35] A.N. Ioannisian, N.A. Kazarian, A.Y. Smirnov and D. Wyler, *A precise analytical description of the earth matter effect on oscillations of low energy neutrinos*, *Phys. Rev.* **D 71** (2005) 033006 [hep-ph/0407138];
E.K. Akhmedov, M.A. Tortola and J.W.F. Valle, *A simple analytic three-flavour description of the day-night effect in the solar neutrino flux*, *JHEP* **05** (2004) 057 [hep-ph/0404083].

[36] M. Blennow and T. Ohlsson, *Effective neutrino mixing and oscillations in dense matter*, *Phys. Lett.* **B 609** (2005) 330 [hep-ph/0409061].

[37] T. Ohlsson and W. Winter, *Reconstruction of the Earth's matter density profile using a single neutrino baseline*, *Phys. Lett.* **B 512** (2001) 357 [hep-ph/0105293];
W. Winter, *Probing the absolute density of the Earth's core using a vertical neutrino beam*, *Phys. Rev.* **D 72** (2005) 037302 [hep-ph/0502097];
H. Minakata and S. Uchinami, *On in situ determination of Earth matter density in neutrino factory*, *Phys. Rev.* **D 75** (2007) 073013 [hep-ph/0612002];
R. Gandhi and W. Winter, *Physics with a very long neutrino factory baseline*, *Phys. Rev.* **D 75** (2007) 053002 [hep-ph/0612158].

[38] P. Lipari (1998) unpublished;
T. Kajita, *Atmospheric neutrinos*, *New J. Phys.* **6** (2004) 194.

[39] E.Kh. Akhmedov, M. Maltoni and A.Yu. Smirnov, in preparation.

[40] E.K. Akhmedov, P. Huber, M. Lindner and T. Ohlsson, *T violation in neutrino oscillations in matter*, *Nucl. Phys.* **B 608** (2001) 394 [hep-ph/0105029].

[41] A.M. Dziewonski and D.L. Anderson, *Preliminary reference Earth model*, *Phys. Earth Planet. Interiors* **25** (1981) 297.

[42] J. Bouchez et al., *Matter effects for solar neutrino oscillations*, *Z. Physik* **C 32** (1986) 499;
V.K. Ermilova, V.A. Tsarev, V.A. Chechin, *Buildup of neutrino oscillations in the Earth*, *Sov. Phys. JETP* **43** (1986) 453 [*Zh. Eksp. Teor. Fiz.* **43** (1986) 353];
A.Y. Smirnov, *The MSW effect and matter effects in neutrino oscillations*, *Phys. Scripta* **121** (2005) 57 [hep-ph/0412391].

JHEP05(2007)077

Received: *April 25, 2008*

Erratum

The correct address of the Instituto de Física Teórica is:

Instituto de Física Teórica UAM-CSIC, Facultad de Ciencias C-XVI,
Universidad Autónoma de Madrid, Cantoblanco, Madrid 28049, Spain

JHEP05(2007)077